APPLIED PHYSICS REVIEWS—FOCUSED REVIEW

Vibrational lifetimes of hydrogen in silicon

G. Lüpke[a)]
Department of Applied Science, The College of William & Mary, Williamsburg, Virginia 23187

N. H. Tolk and L. C. Feldman
Department of Physics and Astronomy, Vanderbilt University, Nashville, Tennessce 37235

(Received 2 July 2002; accepted 14 August 2002)

Characterization of defect and impurity reactions, dissociation, and migration in semiconductors requires a detailed understanding of the rates and pathways of vibrational energy flow, of the energy transfer channels, and of the coupling mechanisms between local modes and the phonon bath of the host material. Significant progress in reaching this goal has been accomplished in recent landmark studies exploring the excitation and dynamics of vibrational states associated with hydrogen in silicon. The lifetime of the Si–H stretch mode is found to be extremely dependent on the local solid-state structure, ranging from picoseconds for interstitial-like hydrogen, hundreds of picoseconds for hydrogen–vacancy complexes, to several nanoseconds for hydrogen bonded to Si surfaces—over three orders of magnitude variation. Such large variations in lifetime (transition probability) are extraordinarily rare in solid-state science. The level of theoretical investigation into the vibrational lifetime of the Si–H oscillator is less advanced. This state of affairs is partly because of the difficulties in explicitly treating slow relaxation processes in complex systems, and partly because, as suggested by experiment, a highly anharmonic coupling mechanism is apparently responsible for the (multiphonon) relaxation process. Even more importantly, because of the high frequency of the Si–H stretching motion, a quantum mechanical treatment of the Si–H oscillator is required. A combination of Bloch–Redfield theory and molecular dynamics simulation seems promising in describing the relaxation process of the Si–H vibrational modes. It is the aim of this review article to present a comprehensive overview of the recent accomplishments, current understandings, and future directions in this emerging field of time-resolved vibrational spectroscopy of point defects in solids. © *2003 American Institute of Physics.*
[DOI: 10.1063/1.1517166]

TABLE OF CONTENTS

I. INTRODUCTION . . . 2317
II. THEORY . . . 2318
A. Bloch–Redfield theory . . . 2319
B. Vibrational relaxation and pure dephasing . . . 2320
C. Multiphonon relaxation . . . 2320
D. System-field interaction . . . 2321
III. EXPERIMENT . . . 2322
A. Pump–probe technique . . . 2322
B. Transient-grating method . . . 2323
C. Time-resolved sum–frequency generation . . . 2323
D. Infrared absorption spectroscopy . . . 2324
IV. CRYSTALLINE SILICON . . . 2324
A. Bond-center hydrogen . . . 2325
B. Structural dependence . . . 2326
C. Decay channels . . . 2327
D. Deuterium lifetimes . . . 2328
V. AMORPHOUS SILICON . . . 2329
A. Hydrogen stretch band . . . 2329
B. Molecular dynamics simulations . . . 2330
VI. SILICON SURFACES . . . 2331
A. Si(111):H Surface . . . 2331
B. Si(100):H Surface . . . 2332
C. Theoretical results . . . 2333
VII. CONCLUSIONS AND OUTLOOK . . . 2334

I. INTRODUCTION

Study of the relaxation dynamics of local vibrational modes (LVMs) in semiconductors down to the picosecond time scale is an emerging field. Direct time-domain measurements of the lifetime of LVMs is made possible by recent advances in tunable, ultrafast, high-intensity infrared (IR) light sources, including optical parametric amplifiers (OPAs) (Refs. 1 and 2) and free-electron lasers (FELs).[3,4] Such studies allow the elucidation of the nature and pathways of energy transfer at defects and impurities in semiconductors under dynamical conditions. The coupling between LVMs and the heat (phonon) bath is responsible for the flow of energy

[a)]Electronic mail: luepke@jlab.org

 © 2003 American Institute of Physics

Downloaded 24 May 2004 to 129.59.117.76. Redistribution subject to AIP license or copyright, see http://jap.aip.org/jap/copyright.jsp

into and out of impurity and defect complexes. This is important, because when defects act as recombination or scattering centers in semiconductors, the electronic excitation that is deposited at the defects is then available to promote defect migration and reactions, an area of defect physics that has an important impact on the degradation of electronic and photonic devices. Hence, a better understanding of the physical properties of defects and impurities in semiconductors can be obtained by studying the dynamics of the elastic and inelastic local interactions.

Information on the inelastic microscopic interactions can be obtained from the lifetime of LVMs. Vibrational energy relaxation in condensed phases entails the redistribution of the excess energy into low-frequency (often vibrational) degrees of freedom that are anharmonically coupled to the initially excited local mode. These inelastic interactions of an oscillator with the low-frequency modes result in energy relaxation times that are typically hundreds of femtoseconds to hundreds of picoseconds in solids.[5–10] The energy relaxation lifetime most often cannot be derived from the linewidth of the linear absorption spectrum.[11,12] This is due to the fact that generally elastic interactions leading to dephasing of the vibrational transition and the associated line broadening (pure dephasing) occur on even shorter time scales.[13–16] Furthermore, inhomogeneous effects may contribute significantly to the observed absorption linewidth. Therefore time-domain, nonlinear spectroscopic experiments, such as pump–probe saturation spectroscopy, are necessary to obtain information on the vibrational population lifetime.

Light impurities in semiconductors, such as hydrogen and deuterium, give rise to localized vibrational modes with frequencies above the phonon bands of the solid.[17] The vibrational spectroscopy of these high-frequency modes has become an important probe of defects in solids and often provides information about defect structure and properties that cannot be obtained by other methods.[18] LVM spectroscopy has been applied extensively to study isolated impurities and impurity complexes in crystalline solids, including ionic crystals[17] and semiconductors.[18] One of the impurity-materials systems studied most extensively by LVM spectroscopy is H in semiconductors, which has attracted much interest because of hydrogen's ability to interact with virtually any lattice imperfection, including impurities, intrinsic defects, surfaces, and interfaces, thus possibly changing the electronic properties of the material.[19,20] Until now, most spectroscopic studies of H-related LVMs in semiconductors have been carried out in the frequency domain, which probes the time-averaged optical response of the modes. Consequently, very little is known about the dynamics of these modes, i.e., the time scales and mechanisms for population and phase relaxation upon excitation. Such information is crucial since excited vibrational states may be involved in the dissociation of the bond between H and the lattice. For instance, Persson, Avouris, Lyding, and their co-workers have reported intriguing data on the different behaviors of the desorption of deuterium (D) and H bonded to Si.[21–24] Although the chemical binding of these species is essentially the same, the difference in desorption behavior was attributed to differences in their vibrational lifetimes.[25] To understand such processes, it is necessary to know the time scale on which excited vibrational states decay, which is given by the lifetime of the states.

The aim of this review article is to present a comprehensive overview of the recent theoretical and experimental results with respect to the vibrational lifetimes of hydrogen and deuterium-related modes in silicon. Theoretical results have been obtained with a method that combines Bloch–Redfield theory and molecular dynamics (MD) simulations. This approach is described in the theory section (Sec. II A). A theoretical description of vibrational relaxation and dephasing processes is outlined in Sec. II B. Given the general importance of multiphonon relaxation for the lifetime of LVMs, a theory of relaxation rates based on a microscopic Hamiltonian is presented in Sec. II C. The interaction between the system and the radiation field is briefly described in the last theory section (Sec. II D).

The various experimental techniques used to measure vibrational lifetimes are presented in Sec. III. The pump–probe transient bleaching technique is the most common time-resolved method for vibrational lifetime measurements (Sec. III A). The transient-grating method belongs to the same class of degenerate four-wave-mixing techniques as the pump–probe method, but allows for background-free detection, which may increase the signal-to-noise ratio in lifetime measurements (Sec. III B). Lifetime measurements of adsorbates on surfaces require a time-resolved surface-sensitive technique such as IR sum–frequency generation (SFG). A simple combination of SFG and transient bleaching is described in Sec. III C. The lifetime of LVMs can also be studied in the frequency domain by infrared absorption spectroscopy (IRAS) (Sec. III D).

The remainder of this review article consists of three sections presenting experimental results of the lifetime of the Si–H stretch mode in different environments, including crystalline Si (Sec. IV), hydrogenated amorphous Si (Sec. V), and hydrogen adsorbed on a Si surface (Sec. VI). Section IV reviews recent lifetime measurements of H-related defects in crystalline silicon, including bond-center hydrogen (Sec. IV A), the structural dependence for different H-related defects (Sec. IV B), their decay channels (Sec. IV C), and their relationship to deuterium lifetimes (Sec. IV D). Section V reviews lifetime studies in amorphous silicon (*a*-Si). The results of pump–probe and transient-grating experiments are presented in Sec. V A. Section V B reports MD simulations of vibrational lifetimes of local and extended modes in *a*-Si. The last experimental section (Sec. VI) reviews the vibrational lifetimes of the Si–H stretch mode on Si surfaces. Sections VI A and VI B present lifetime data from H:Si(111) and H:Si(100) surfaces, respectively. Theoretical results for the vibrational lifetimes of the hydrogen stretch mode on Si surfaces are reported in Sec. VI C. The article concludes with a brief summary and an evaluation of future directions (Sec. VII).

II. THEORY

The level of theoretical investigation into the vibrational lifetime of the Si–H oscillator is less advanced. This state of

Downloaded 24 May 2004 to 129.59.117.76. Redistribution subject to AIP license or copyright, see http://jap.aip.org/jap/copyright.jsp

affairs is partly because of the difficulties in explicitly treating slow relaxation processes in complex systems, and partly because, as suggested by experiment, a highly anharmonic coupling mechanism is apparently responsible for the relaxation process. Even more importantly, because of the high frequency of the Si–H stretching motion, results from a classical treatment of the Si–H oscillators may not be particularly accurate. Bloch–Redfield theory provides the quantum mechanical equations of motion of the density operator of a system (local oscillator) in contact with a thermal bath. Expressions for the vibrational relaxation and dephasing rates are derived by defining an effective vibrational Hamiltonian that represents canonical averages over the bath modes. By expanding the system–bath-interaction Hamiltonian to high order in the phonon coordinates an expression for the multiphonon relaxation rate is derived. A theoretical description of the interaction between the system and an incoming laser pulse is presented in the last part of this section.

A. Bloch–Redfield theory

Theoretical results have been obtained with a method that combines Bloch–Redfield theory and molecular dynamics simulations.[26–29] The Bloch–Redfield theory component allows one to treat the multilevel population evolution of a high-frequency Si–H oscillator in a quantum mechanical fashion. The molecular dynamics component, on the other hand, allows one to treat the interaction of the Si–H stretch with the vibrational degrees of freedom of the bath for a high level of complexity.

A brief description of the Bloch–Redfield theory is given here as it applies to the vibrational energy relaxation dynamics of the Si–H oscillator. The total Hamiltonian is written as follows:

$$H(q,Q)=H_S(Q)+H_B(q)+H_I(q,Q), \tag{1}$$

where Q and q represent the coordinates of the quantum Si–H oscillator and the bath, respectively. H_S is the Hamiltonian for the vibrational levels of the system (Si–H bond), H_B is the Hamiltonian of the bath (phonons), and H_I is the interaction between the LVM and the phonon bath. Typically, the system contains a few degrees of freedom of interest, Q, whereas the bath consists of many degrees of freedom, q. The total density operator in the joint system and bath phase space is too complex and cannot be calculated explicitly.

Bloch–Redfield theory utilizes an important advantage of the density operator, namely, that it offers the possibility to describe only a part of the system of interest, i.e., it provides a reduced description. In this approach,[26,30,31] one assumes that the state of the bath can be well described at all times by a fixed, thermal equilibrium density matrix, and derives an equation for the "reduced density matrix" of the Q system, which involves some correlation functions of operators mixing the Q system and the bath. Assuming the total density matrix at $t=0$ can be written $\sigma(0)=\rho(0)\rho_B$, where the bath density operator is given by $\rho_B=\exp[-\beta H_B/Tr(-\beta H_B)]$, with $\beta=(k_BT)^{-1}$. The density matrix elements of the system in interaction with the thermal bath obey the equations of motion[32]

$$\dot{\rho}_{\alpha\beta}(t)=-i\omega_{\alpha\beta}\rho_{\alpha\beta}(t)-\sum_{\alpha',\beta'}R_{\alpha\beta,\alpha'\beta'}\rho_{\alpha'\beta'}(t), \tag{2}$$

where $\rho_{\alpha\beta}(t)$ is the reduced density matrix element and $\omega_{\alpha\beta}=(E_\alpha-E_\beta)/\hbar$ is the frequency of oscillation of coherence between the eigenstates $|\alpha\rangle$ and $|\beta\rangle$ of the system. The first term on the right-hand side of Eq. (2) describes the unperturbed motion of the system as determined by its Hamiltonian H_S. The matrix R describes the relaxation of the system by the statistical perturbation $H_I(t)$. It will be called the "relaxation matrix." The elements of the Redfield tensor have a straightforward interpretation. $R_{\alpha\beta,\alpha'\beta'}$ is a rate constant for the process $\rho_{\alpha\beta}\rightarrow\rho_{\alpha'\beta'}$. If $\alpha=\alpha'$ and $\beta=\beta'$, this is a dephasing rate for the coherence $\rho_{\alpha\beta}$. If $\alpha=\beta$ and $\alpha'=\beta'$, then the term represents a population relaxation rate between eigenstates $|\alpha\rangle$ and $|\alpha'\rangle$ of the system. Other terms describe the coupling between populations and coherences and coherence transfer. The relaxation matrix $R_{\alpha\beta,\alpha'\beta'}$ is given by[26–29]

$$R_{\alpha\beta,\alpha'\beta'}=-\delta_{\beta'\beta}\sum_\gamma\Gamma^+_{\alpha\gamma,\gamma\alpha'}-\delta_{\alpha\alpha'}\sum_\gamma\Gamma^-_{\beta'\gamma,\gamma\beta}+\Gamma^+_{\beta'\beta,\alpha\alpha'}+\Gamma^-_{\beta'\beta,\alpha\alpha'}, \tag{3}$$

$$\hbar^2\Gamma^+_{\beta'\beta,\alpha\alpha'}=\langle\beta'|q|\beta\rangle\langle\alpha|q|\alpha'\rangle\times\int_0^\infty dt e^{-i\omega_{\alpha\alpha'}t}\langle F(t)F(0)\rangle, \tag{4}$$

$$\hbar^2\Gamma^-_{\beta'\beta,\alpha\alpha'}=\langle\beta'|q|\beta\rangle\langle\alpha|q|\alpha'\rangle\times\int_0^\infty dt e^{-i\omega_{\beta'\beta}t}\langle F(0)F(t)\rangle. \tag{5}$$

In Eqs. (3)–(5), $\langle\alpha|q|\alpha'\rangle$ is the transition matrix element between eigenstates $|\alpha\rangle$ and $|\alpha'\rangle$, $\delta_{\alpha\alpha'}$ is the Kronecker delta, and the dynamical function $F(t)$ is the classical fluctuating force on the Si–H bond arising from the coupling to the other modes of the system. In the derivation of Eq. (2) many assumptions have been made:[30,31] (1) The interaction Hamiltonian can be written as $H_I(t)=qF(t)$, which is to be computed with the oscillator frozen at its equilibrium position. (2) The thermal bath remains in thermal equilibrium. (3) The relaxation times of the system under study are much longer than the autocorrelation time τ_c of the force. The first assumption is mostly of a technical nature and represents no problem if the coupling is small. The second assumption is reasonable because the amount of energy transferred to the bath is small and also because the many-body bath can reestablish equilibrium quickly. The third assumption can be checked self-consistently by performing the MD simulations.

The correlation functions appearing in the expressions for $\Gamma^\pm$ are quantum mechanical. Replacing them by their classical limit violates detailed balance and does not lead to thermodynamic equilibrium.[33] To go smoothly to the classical limit one rewrites them in terms of the symmetrized correlation function, which is then replaced by the classical autocorrelation function, which can be computed by means of MD.[33] Bloch–Redfield theory seems promising in describing vibrational relaxation processes.

Downloaded 24 May 2004 to 129.59.117.76. Redistribution subject to AIP license or copyright, see http://jap.aip.org/jap/copyright.jsp

B. Vibrational relaxation and pure dephasing

The vibrational Hamiltonian, $H(q,Q)$, is a multidimensional operator that describes the static and dynamic properties of the vibrational states. We can formally reduce it to a one-dimensional effective Hamiltonian by defining a new operator that represents a canonical average over the bath modes. Let

$$H(Q)=\langle H(q,Q)\rangle, \tag{6}$$

$$V(q,Q)=H(q,Q)-H(Q), \tag{7}$$

where $V(q,Q)$ represents fluctuations of this operator from its canonical average. Expanding $V(q,Q)$ to second order in the system coordinate about the equilibrium position Δ gives

$$V(q,Q)=V(q,\Delta)+\left.\frac{\partial V}{\partial Q}\right|_{\Delta}(Q-\Delta)+\frac{1}{2}\left.\frac{\partial^2 V}{\partial Q^2}\right|_{\Delta}(Q-\Delta)^2. \tag{8}$$

The zeroth-order term does not depend on Q and is thus included in the bath Hamiltonian. The displaced oscillator states will be denoted by Greek letters with a prime. In terms of the displaced oscillator states, the operator describing the system–bath interaction becomes

$$H_I=\sum_{\alpha'\beta'}\phi_{\alpha'\beta'}P_{\alpha'\beta'}, \tag{9}$$

where $\phi_{\alpha'\beta'}=\langle\alpha'|V(q,Q)|\beta'\rangle$ are elements of the fluctuation matrix, and $P_{\alpha'\beta'}=|\alpha'\rangle\langle\beta'|$ are the vibrational operators.

Assuming that the coupling between the system coordinate and the bath is sufficiently weak, the rate constant, $\Gamma_{\alpha'\beta'}$, for population relaxation from vibrational state α' to β' can be written as a Fourier transform of the autocorrelation function of the appropriate fluctuation matrix elements:[34,35]

$$\Gamma_{\alpha'\beta'}=1/T_1=h^{-2}\int_{-\infty}^{\infty}dt\,e^{i\omega_{\alpha'\beta'}t}\langle\phi_{\alpha'\beta'}(t)\phi_{\alpha'\beta'}(0)\rangle, \tag{10}$$

where $\phi_{\alpha'\beta'}(t)=\exp(iH_Bt)\phi_{\alpha'\beta'}(0)\exp(-iH_Bt)$. The correlation function appearing in Eq. (10) involves only the bath variables and is assumed to decay exponentially with a time constant τ_c, the bath correlation time.

Coherent excitation results in a phase coherence between the vibrational states, $\rho_{\alpha'\beta'}(t)$, which gives rise to a macroscopic vibrational amplitude. In the absence of population relaxation, the phase coherence described by $\rho_{\alpha'\beta'}(t)$ will, in the Bloch approximation, decay exponentially with a time constant T_2^*. Again, perturbation theory gives the result

$$\Gamma^*_{\alpha'\beta'}=1/T_2^*=h^{-2}/2\int_{-\infty}^{\infty}dt\langle[\phi_{\alpha'\alpha'}(t)-\phi_{\beta'\beta'}(t)]\times[\phi_{\alpha'\alpha'}(0)-\phi_{\beta'\beta'}(0)]\rangle. \tag{11}$$

The total dephasing rate between two levels is given by

$$\Gamma_{\alpha'\beta'}=\sum_{\gamma'}\Gamma_{\alpha'\gamma'}+\sum_{\gamma'}\Gamma_{\beta'\gamma'}+\Gamma^*_{\alpha'\beta'}, \tag{12}$$

where the summations denote the sum of all the T_1 processes originating in states α' and β'. The theory outlined above, in which the bath is described by fluctuation operators, provides a convenient way to calculate the various relaxation rates.

C. Multiphonon relaxation

If the vibrational relaxation process involves transfering energy directly to the bath modes (phonons) in a single step, and the amount of energy transferred exceeds by many times the maximum energy of a single phonon, then many phonons will have to be created simultaneously. This process is known as multiphonon relaxation. One might reasonably imagine that the rate of such a high-order process would be quite small. Therefore, it is remarkable that even if the number of phonons emitted is as high as ten or more, multiphonon processes typically compete successfully with radiative decay, and are in fact often the dominant relaxation mechanism.[36–51]

Given the general importance of multiphonon relaxation, it is clearly desirable to develop a theory of relaxation rates based on a microscopic Hamiltonian. Existing theories involve one of two approaches: the adiabatic (Born–Oppenheimer) or "static-coupling" (crude Born–Oppenheimer) methods. The first method is usually invoked when discussing relaxation between electronic states, but can be applied to high-frequency vibrations as well. The coordinates are divided into fast (electronic or high-frequency vibration) and slow (phonon) components. One neglects for the moment the kinetic energy of the phonons, and finds the eigenstates of the Hamiltonian for fixed phonon coordinates. The eigenvalues of this procedure generate the usual adiabatic potential surfaces, and transitions between these surfaces are due to the "nonadiabatic" coupling (phonon kinetic energy) term in the full Hamiltonian. Even when this nonadiabatic coupling is taken to lowest order in perturbation theory, multiphonon transitions emerge. This was the approach pioneered by Kubo and Toyozawa,[52] Perlin,[53] Miyakawa and Dexter,[54] and others.[55–60]

The second approach goes by several different names but its essence is as follows: one assumes that the Hamiltonian can be written as

$$H=H_S+H_B+H_I. \tag{13}$$

The Hamiltonian of the local vibrational mode,

$$H_S=\hbar\omega a^{\dagger}a, \tag{14}$$

is characterized in terms of the frequency ω, creation operator $a^{\dagger}$, and annihilation operator a. The (harmonic) Hamiltonian for the phonon bath is given by

$$H_B=\sum_k\hbar\omega b_k^{\dagger}b_k, \tag{15}$$

where $b_k^{\dagger}$ and b_k are the phonon creation and annihilation operators, respectively. There are at least three different possible routes to multiphonon relaxation based on the form of the interaction Hamiltonian H_I.[61] In the most common approach H_I is strictly off-diagonal in the two-level basis of the

Downloaded 24 May 2004 to 129.59.117.76. Redistribution subject to AIP license or copyright, see http://jap.aip.org/jap/copyright.jsp

local vibrational mode.[61,62] The off-diagonal matrix elements of H_I are expanded to high order in the phonon coordinates, and are treated by lowest-order time-dependent perturbation theory. The interaction Hamiltonian is then given by

$$H_I=\sum_{\{\nu\}} \hbar(G_{\{\nu\}}B_{\{\nu\}}a^\dagger+G^*_{\{\nu\}}B^\dagger_{\{\nu\}}a), \tag{16}$$

where $B_{\{\nu\}}=\Pi_{i=1}^{N_\nu}b_{i,\{\nu\}}$, $B^\dagger_{\{\nu\}}=\Pi_{i=1}^{N_\nu}b^\dagger_{i,\{\nu\}}$, and $G_{\{\nu\}}$ denotes the temperature-independent coupling strength of the channel $\{\nu\}$. $\{\nu\}$ is characterized by the set $\{\omega_1^{(\nu)},\omega_2^{(\nu)},\ldots,\omega_{N_\nu}^{(\nu)},\}$ of accepting mode frequencies. Energy is conserved in the decay process, $\hbar\omega=\Sigma_{j=1}^{N_\nu}\hbar\omega_j^{(\nu)}$. The contribution to the decay rate due to H_I is given by the standard result of first-order time-dependent perturbation theory.[63] The total decay rate (inverse lifetime) is given as the sum of the rates of all of the decay channels:[61,62]

$$\frac{1}{T_1}=2\pi\sum_{\{\nu\}} |G_{\{\nu\}}|^2 n_{\{\nu\}}\rho_{\{\nu\}}. \tag{17}$$

The function $n_{\{\nu\}}$ describes the temperature-dependent population of the receiving modes:

$$n_{\{\nu\}}=\frac{\exp(\beta\hbar\omega)-1}{\Pi_{j=1}^{N_\nu}[\exp(\beta\hbar\omega_j^{(\nu)})-1]}. \tag{18}$$

The compound spectral density of accepting states, $\rho_{\{\nu\}}$, can be expressed in terms of a convolution of single spectral densities of states:

$$\rho_{\{\nu\}}=\int d\omega_1^{(\nu)}\cdots\int d\omega^{(\nu)}_{(N_\nu-1)}\rho_1^{(\nu)}(\omega_1^{(\nu)})\cdots\rho^{(\nu)}_{N_\nu}(\omega^{(\nu)}_{N_\nu}). \tag{19}$$

In the low-temperature limit ($k_BT\ll\hbar\omega_j^{(\nu)}$, for all j), the decay rate reflects spontaneous decay into N_ν accepting modes and $n_{\{\nu\}}\cong 1$. At higher temperatures the decay rate increases due to stimulated emission in a fashion determined by the frequencies of the accepting modes.[61,62] As a rule, the process with the least amount of phonons should be favored.

D. System–field interaction

In conventional relaxation theories for excited states, the assumption of fast dissipation results in dynamics that are insensitive to the nature of the prepared state. For cases where either population relaxation and/or pure dephasing occurs on a time scale comparable to (or longer than) the initial vibrational excitation, this is not necessarily true. In these cases one must explicitly take into account the frequency and temporal properties of the excitation pulse. The interaction between the system and an incoming laser pulse is given by

$$H_{SF}(t)=-\mu E(t), \tag{20}$$

where μ is the transition dipole operator and $E(t)$ is the time-dependent electric field, which can be written as

$$E(t)=E_0(t)\exp(i\omega_L t), \tag{21}$$

where $E_0(t)$ is the temporal profile of the pulse and ω_L the center frequency. Assuming the excitation pulse is a transform-limited pulse from a mode-locked laser, the spectral width is determined by the Fourier transform of $E_0(t)$.

We assume that only the first excited state $|\beta\rangle$ is optically accessible from the ground state $|\alpha\rangle$ of the system, so that the transition dipole operator has the form

$$\mu=\mu_{\alpha\beta}\{|\alpha\rangle\langle\beta|+|\beta\rangle\langle\alpha|\}, \tag{22}$$

where the matrix elements of the transition dipole operator have the form $\mu_{\alpha\beta}=\langle\alpha|\hat{\mu}|\beta\rangle$. For simplicity, we will assume there is no dissipation in the system during the excitation pulse. The validity of this approximation for any given pulse duration will obviously depend on the magnitude of the fluctuations. In the absence of dissipation, the dynamics of the density matrix is governed by the quantum mechanical Liouville equation

$$\frac{\partial\rho(t)}{\partial t}=-\frac{i}{\hbar}[H+H_{SF}(t),\rho(t)]. \tag{23}$$

In order to solve the Liouville equation, the time-dependent perturbation theory with the perturbation Hamiltonian $H_{SF}(t)$ has been used to calculate the nth-order density operator.[64] Here, we consider the rate equation description of the density matrix elements to describe the evolution of the nonequilibrium state.

We assume that the frequency of the excitation pulse, ω_L, is tuned in resonance with the one-quantum vibrational transition between $|\alpha\rangle$ and $|\beta\rangle$ states, i.e., $\omega_L=\omega_{\alpha\beta}$. Due to the resonance enhancement, the vibrational transition from $|\alpha\rangle$ to the other state $|\gamma\rangle$ ($\neq|\beta\rangle$) can be ignored. Also, for the sake of simplicity it is assumed that due to the anharmonicity of the βth mode the transition from $|\beta\rangle$ to $|2\beta\rangle$, where $|2\beta\rangle$ denotes the overtone state, is negligibly small in comparison to the transition probability from $|\alpha\rangle$ to $|\beta\rangle$—note that this two-state assumption is, however, not entirely necessary to develop a theory of the equations of motion of the nonequilibrium density operator. We next consider the equations of motion of the density operator:[65]

$$\dot{\rho}_{\alpha\beta}=-i\omega_{\alpha\beta}\rho_{\alpha\beta}+\frac{i}{\hbar}E(t)\mu_{\alpha\beta}(\rho_{\beta\beta}-\rho_{\alpha\alpha})-\Gamma_{\alpha\beta}\rho_{\alpha\beta}, \tag{24}$$

$$\dot{\rho}_{\beta\alpha}=i\omega_{\alpha\beta}\rho_{\alpha\beta}-\frac{i}{\hbar}E(t)\mu_{\beta\alpha}(\rho_{\beta\beta}-\rho_{\alpha\alpha})-\Gamma_{\alpha\beta}\rho_{\beta\alpha}, \tag{25}$$

$$\dot{\rho}_{\alpha\alpha}=-\frac{i}{\hbar}E(t)(\mu_{\alpha\beta}\rho_{\beta\alpha}-\mu_{\beta\alpha}\rho_{\alpha\beta})-\gamma_\alpha\rho_{\alpha\alpha}+\gamma_\beta\rho_{\beta\beta}, \tag{26}$$

$$\dot{\rho}_{\beta\beta}=\frac{i}{\hbar}E(t)(\mu_{\alpha\beta}\rho_{\beta\alpha}-\mu_{\beta\alpha}\rho_{\alpha\beta})+\gamma_\alpha\rho_{\alpha\alpha}-\gamma_\beta\rho_{\beta\beta}, \tag{27}$$

where γ_α and γ_β represent population relaxation (T_1) rates and $\Gamma_{\alpha\beta}$ is the dephasing (T_2) rate. In Eqs. (24)–(27), the vibrational population transfer from $|\alpha\rangle$ to $|\beta\rangle$ states is fully described by the time-dependent pump–pulse-induced transition rate, $\Omega(t)$, which is given as[66]

$$\Omega(t)\equiv\frac{2\pi}{\hbar^2}|\mu_{\alpha\beta}E(t)|^2 g_{\alpha\beta}(\omega), \tag{28}$$

Downloaded 24 May 2004 to 129.59.117.76. Redistribution subject to AIP license or copyright, see http://jap.aip.org/jap/copyright.jsp

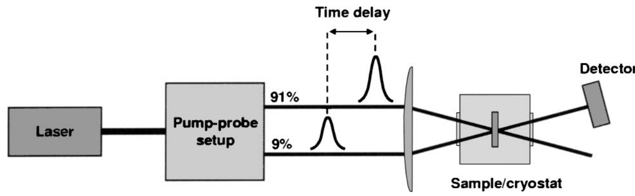

FIG. 1. Schematic of the pump–probe transient bleaching setup.

where the line-shape function, $g_{\alpha\beta}(\omega)$, is assumed to be a Lorentzian function:

$$g_{\alpha\beta}(\omega)=\frac{\Gamma_{\alpha\beta}}{\pi[(\omega-\omega_{\alpha\beta})^2+\Gamma_{\alpha\beta}^2]}. \tag{29}$$

The solution of Eqs. (24)–(27) can be used to describe the time evolution of the nonequilibrium density operator $\rho_{\mathrm{Neq}}(t)$. The preparation step of the nonequilibrium state was treated nonperturbatively. However, one can use second-order (with respect to the pump IR field) perturbation theory to obtain $\rho_{\mathrm{Neq}}(t)$, if the pump intensity is not too large. Next, we consider the probe–field–matter interaction Hamiltonian, which is given by

$$H_{SP}(t)=-\mu\cdot E_{\mathrm{pr}}(t), \tag{30}$$

where $E_{\mathrm{pr}}(t)$ is the electric field of the infrared probe pulse which peaks at $t=\tau$. The density operator at time τ is given by

$$\rho_{\mathrm{Neq}}^{(1)}(\tau)\simeq\rho_{\mathrm{eq}}-\frac{i}{\hbar}\int_0^\tau dt[H_{SP}(t),\rho_{\mathrm{Neq}}(t)]. \tag{31}$$

Even though the pump field is assumed to be strong, the probe field is weak, and therefore the perturbation approach is quantitatively acceptable. In Eq. (31), the second term corresponds to the first-order (with respect to the infrared probe field) contribution to the density operator. The nonequilibrium polarization, which is defined as the dipole moment averaged over the nonequilibrium density operator, is given by

$$P_{\mathrm{Neq}}(t)=\langle\mu\rho_{\mathrm{Neq}}^{(1)}(t)\rangle. \tag{32}$$

Finally, the weak probe absorption signal can be calculated, within the slowly varying-amplitude approximation, as

$$S_b(\tau)=\frac{4\pi\omega_{\alpha\beta}}{cn(\omega_{\alpha\beta})}\,\mathrm{Im}\int_0^\tau dtE_{\mathrm{pr}}^*(t)P_{\mathrm{Neq}}(t)\Big/\int_0^\tau dt|E_{\mathrm{pr}}(t)|^2, \tag{33}$$

where $n(\omega_{\alpha\beta})$ is the index of refraction. The time evolution of $S_b(\tau)$,

$$S_b(\tau)\propto\exp[-\tau/T_1], \tag{34}$$

provides direct information on the vibrational lifetime of the first excited state of the local vibrational mode.

III. EXPERIMENT

In order to observe vibrational lifetimes in semiconductors on the picosecond time scale, several ultrafast optical techniques have been employed. The most common time-domain (pump–probe) measurement techniques include the transient bleaching technique, the transient-grating method, and a combination of sum–frequency generation and transient bleaching. In special cases, the vibrational lifetime can also be obtained in the frequency domain by IR absorption spectroscopy. This section presents a brief description of these optical techniques.

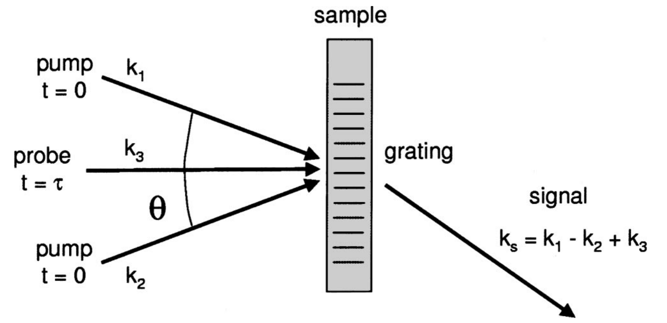

FIG. 2. Schematic of the transient grating experiment.

A. Pump–probe technique

Lifetimes ranging from a few picoseconds to several nanoseconds can be measured directly by the pump–probe transient bleaching technique utilizing ultrashort pulses from a tunable infrared laser. Typically, two different tunable, infrared lasers are used: ultrafast optical parametric amplifiers[1,2] or picosecond free-electron lasers.[3,4] These lasers can deliver pulses with a time duration of ~1 ps, spectral width of ~15 cm^{-1}, and pulse energies of several μJ. Both lasers can in principle be tuned in wavelength between 1–10 μm, thus covering the Si–H stretch vibrations. The major difference between these lasers is the pulse repetition frequency (PRF), which for OPAs is typically limited to a few kHz, whereas FELs can achieve much higher PRFs. For example, the FEL at the Thomas Jefferson National Accelerator Facility (TJNAF) operates at a PRF of 18 MHz. A high PRF and excellent pulse-to-pulse stability are necessary to achieve a high signal-to-noise ratio in pump–probe measurements.

A schematic diagram of a typical setup for a pump–probe transient bleaching experiment is shown in Fig. 1. The laser beam is split into two parts, pump and probe, carrying 91% and 9% of the power, respectively. The two incident ultrashort laser pulses are spatially overlapped on the sample. The pump excites a fraction of the Si–H bonds to the first excited state, which causes a transient increase in the transmission coefficient of the sample that decays over time due to the decay of the excited mode. The time evolution of the transient bleaching signal S_b,

$$S_b(\tau)\propto\exp[-\tau/T_1], \tag{35}$$

is monitored by varying the time delay (τ) between the pump and probe pulses. The signal S_b is detected with an amplified liquid-nitrogen-cooled HgCdTe or InSb detector. To improve the sensitivity of the experiment a lock-in amplifier is utilized along with an optical chopper, which modulates the excitation for phase-sensitive detection.

Downloaded 24 May 2004 to 129.59.117.76. Redistribution subject to AIP license or copyright, see http://jap.aip.org/jap/copyright.jsp

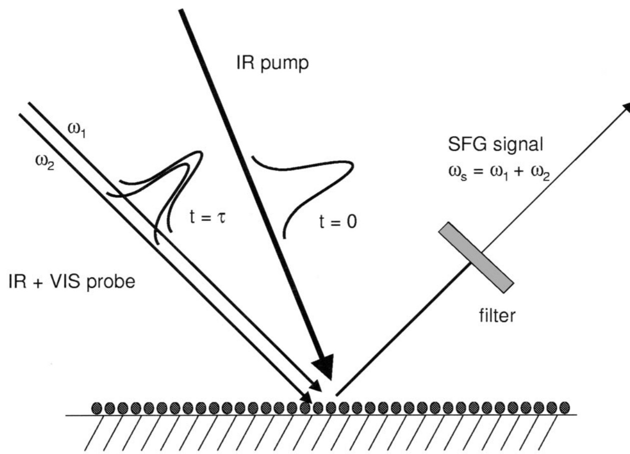

FIG. 3. Schematic of the pump–probe SFG experiment.

B. Transient-grating method

The vibrational lifetime can also be probed by another time-domain technique, transient grating (TG) spectroscopy. The following typical setup is considered (Fig. 2). At time $t=0$ two short excitation pulses, (k_1) and (k_2), are superimposed on the sample under an angle θ, which causes an interference pattern that leads to a spatial modulation of the absorption coefficient, i.e., a transient grating. The decay of the grating as a result of vibrational population relaxation is monitored by applying a probe pulse, (k_3), at time $t=\tau$. The diffracted probe intensity $S_b(\tau)$ decays as

$$S_b(\tau)=\exp[-2\tau/T_1]. \tag{36}$$

Higher signal-to-noise ratios may be obtained with this method than with the pump–probe technique, since the transient-grating signal can be observed in a background-free direction. However, it is necessary to confirm that spatial transport or thermal effects do not affect the decay of the transient-grating signal.

C. Time-resolved sum–frequency generation

Measurements of the vibrational lifetime of Si–H stretch modes on hydrogenated silicon surfaces requires a surface-sensitive time-resolved optical technique. In the past 25 years the nonlinear optical techniques of second-harmonic generation (SHG) and sum–frequency generation have emerged as useful surface probes.[66–69] In SFG, two input laser beams at frequencies ω_1 and ω_2 overlap at the surface and generate a sum–frequency output at $\omega_s=\omega_1+\omega_2$ in both transmitted and reflected directions (Fig. 3). SHG is a special case of SFG with $\omega_1=\omega_2$. The output is highly directional as required by the boundary conditions and can be detected by a photomultiplier through filters and a small monochromator.

The theory of surface SFG has been described in detail elsewhere.[70] We summarize here only the results relevant to the measurements. Both techniques rely on second-order nonlinear-optical processes.[66] In centrosymmetric media, such as silicon, second-order nonlinear processes are forbidden, but at a surface or interface, the inversion symmetry is necessarily broken. This is the basis for the surface sensitivity of SFG and SHG. As an intense electromagnetic field irradiates a material the polarizability that varies linearly for weak fields becomes nonlinear. This leads to various frequency mixing processes. The source of SFG is the nonlinear optical polarization induced in the medium:[66]

$$P(\omega_s)=\chi_s^{(2)}(\omega_s=\omega_1+\omega_2):E(\omega_1)E(\omega_2), \tag{37}$$

where $\chi_s^{(2)}$ is the second-order nonlinear optical susceptibility and $E(\omega_i)$ is the field at ω_i.

A semiclassical perturbative treatment of the interaction between the molecule and the electromagnetic field is required to obtain a complete expression of the nonlinear susceptibility. For SHG, this expression can be found in several publications.[66,71–74] Guyot-Sionnest and co-workers considered the resonant second-order nonlinearity as a perturbation of the molecular polarizability by a normal mode excitation such that[101]

$$P(t)=\left(\alpha_{\text{vis}}^{(1)}+\frac{\partial\alpha_{\text{vis}}^{(1)}}{\partial q}q(t)+\cdots\right)E_{\text{vis}}(t). \tag{38}$$

The IR field $E_{\text{IR}}(t)$ drives the normal mode $q(t)$,

$$q(t)=\Delta\rho\frac{e^*}{m^*}\frac{E_{\text{IR}}(t)}{\omega_0^2-\omega_{\text{IR}}^2-i\omega_{\text{IR}}T_2^{-1}}, \tag{39}$$

where $\Delta\rho$ is the population difference between the ground state and the excited state. The induced polarizability at the sum frequency is then

$$\alpha^{(2)}(\omega=\omega_{\text{IR}}+\omega_{\text{vis}})=\Delta\rho\frac{\partial\alpha_{\text{vis}}^{(1)}}{\partial q}\frac{e^*}{m^*}\frac{1}{\omega_0^2-\omega_{\text{IR}}^2-i\omega_{\text{IR}}T_2^{-1}}. \tag{40}$$

From Eq. (40) it is clear that the mode has to be Raman and IR active to produce SFG. The total surface susceptibility

$$\chi_s^{(2)}=N\langle\alpha^{(2)}\rangle+\chi_{\text{NR}}^{(2)}, \tag{41}$$

contains the resonant contribution of the excited mode, which depends on the molecular coverage N and on the average molecular orientation, and a nonresonant contribution from the adsorbate or the substrate. The SFG signal, $I(\omega_s)$, is proportional to[66]

$$I(\omega_s)\approx|\chi^{(2)}|^2I(\omega_{\text{vis}})I(\omega_{\text{IR}}), \tag{42}$$

where $I(\omega_i)$, $i=s$, IR, vis, is the intensity of the SFG, infrared, and visible pulse. The visible beam energy density is limited by the damage threshold of the substrate. As a consequence, it is advantageous to perform SFG experiments with short (picosecond) pulse laser sources.

Lifetime measurements are performed by a simple combination of SFG and transient bleaching (see Sec. III A). In this scheme, the surface is first excited by an intense infrared beam. This leads to a new population difference $\Delta\rho$ for the adsorbate vibration. The SFG from a delayed pair of a weak infrared beam and a visible beam is then detected. Since the SFG signal is proportional to $(\Delta\rho)^2$ [Eqs. (40)–(42)] it gives directly the ground-state recovery time.

Downloaded 24 May 2004 to 129.59.117.76. Redistribution subject to AIP license or copyright, see http://jap.aip.org/jap/copyright.jsp

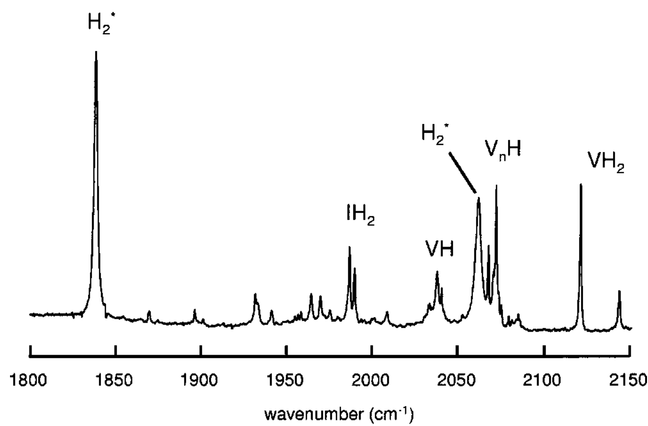

FIG. 4. FTIR spectrum of proton-implanted crystalline silicon.

D. Infrared absorption spectroscopy

The lifetime of LVMs can also be studied in the frequency domain by IRAS. The shape of an absorption line is generally given by the convolution of its homogeneous line shape with a function describing the inhomogeneous broadening.[75] In single crystals, inhomogeneous broadening results from strain fields induced by lattice defects present in the sample. Since the most abundant imperfections in crystalline samples are defects formed during crystal growth or ion implantation, one would expect the inhomogeneous broadening to decrease with decreasing impurity concentration C_I. Generally, the homogeneous line shape is Lorentzian with a full width at half maximum (FWHM) (in cm^{-1}) given by

$$\Gamma_H = \frac{1}{2\pi c T_1} + \frac{1}{\pi c T_2^*}, \tag{43}$$

where T_1 is the lifetime of population (energy) relaxation and T_2^* is the time of phase relaxation (pure dephasing). The first term determines the natural linewidth of the mode, whereas the second term generally dominates the linewidth at elevated temperatures due to elastic scattering of the local mode with phonons. The vibrational lifetime is a good estimate of the natural linewidth.

IV. CRYSTALLINE SILICON

In 1975, Stein reported a pioneering infrared absorption study of crystalline silicon implanted with protons at room temperature (RT).[76] After implantation more than ten absorption lines were observed in the range 1800–2250 cm^{-1} (see Fig. 4). The lines shifted down in frequency by a factor of $1/\sqrt{2}$ when deuterons were implanted instead of protons.

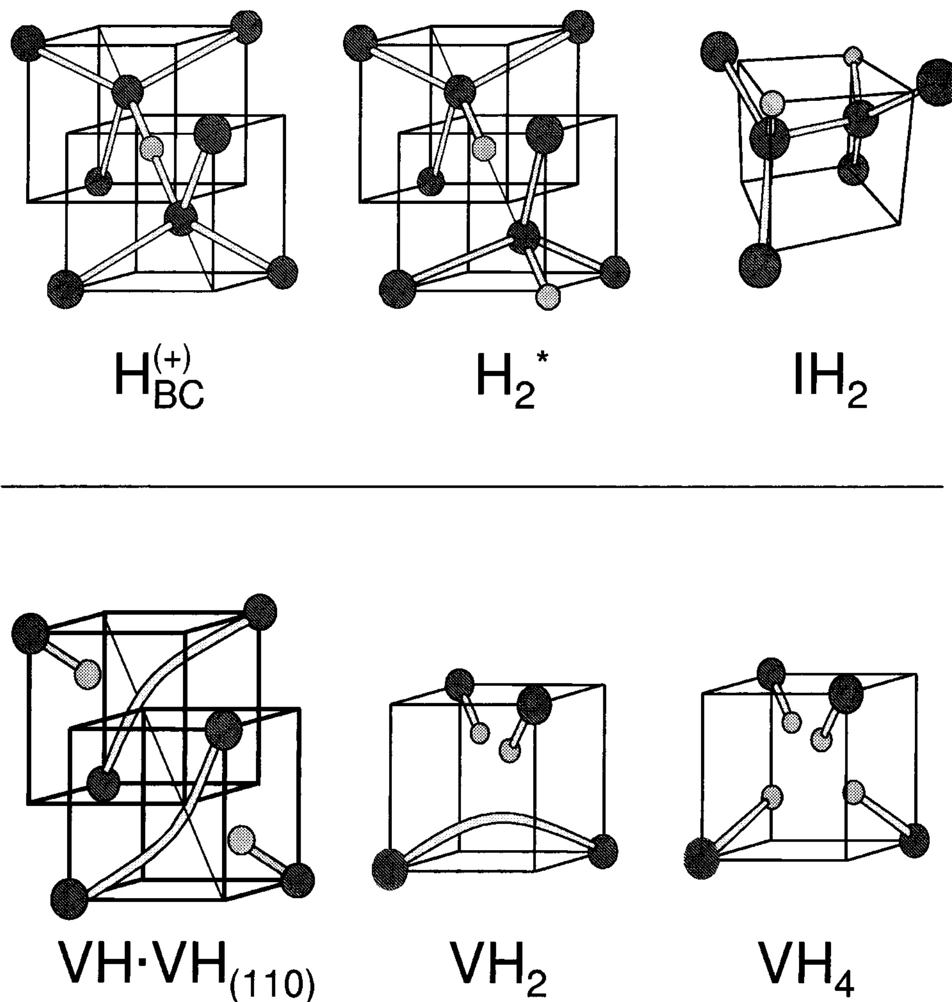

FIG. 5. Structure of the interstitial-type defects (top), and the vacancy-type complexes (bottom). Large spheres are Si, whereas small spheres are H.

Downloaded 24 May 2004 to 129.59.117.76. Redistribution subject to AIP license or copyright, see http://jap.aip.org/jap/copyright.jsp

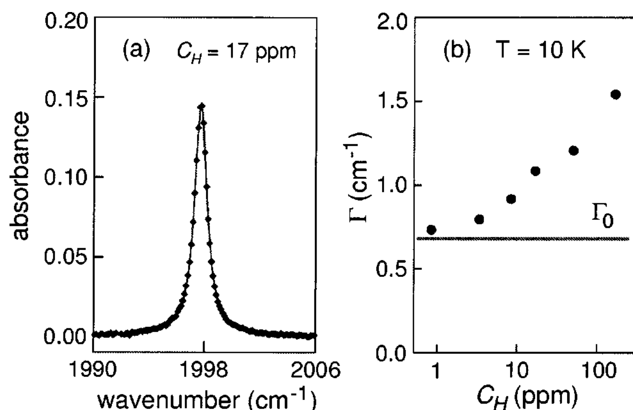

FIG. 6. (a) Absorbance spectrum of proton-implanted Si showing the 1998 cm^{-1} line of $H_{BC}^{(+)}$. Solid line represents a Lorentzian fit to the data. The spectrum was measured at ~10 K on a sample with $C_H = 17$ ppm. (b) FWHM of the 1998 cm^{-1} line vs C_H. The line represents the natural linewidth Γ_0 obtained from the lifetime of the mode and Eq. (44).

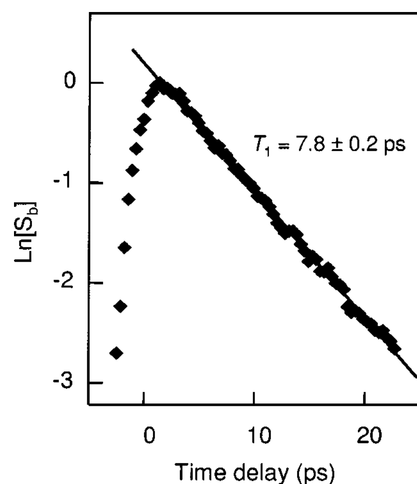

FIG. 7. Decay of the transient bleaching signal from the 1998 cm^{-1} line of $H_{BC}^{(+)}$ measured at ~20 K with the TJNAF FEL.

Based on the observed isotopic shifts and the proximity of the lines to those of Si–H bonds in molecules, Stein assigned the lines to local vibrational stretch modes of Si–H bonds associated with hydrogen-decorated implantation-induced defects (see Fig. 5). Since the original work by Stein, a number of additional Si–H absorption lines have been observed in proton-implanted silicon[77,78] or silicon grown in a H_2 ambient and subsequently irradiated with electrons[79,80] or neutrons.[81] At present, more than 30 distinct absorption lines have been observed in the frequency region associated with Si–H stretch modes. In addition, a number of lines have been observed in the region 550–900 cm^{-1}, which are ascribed to angular vibrations of Si–H bonds.[77,78]

A. Bond-center hydrogen

Recently, Budde and co-workers have performed first transient bleaching experiments of the vibrational lifetime of bond-center hydrogen in crystalline silicon using the FEL at the TJNAF.[82] The lifetime of the stretch mode of bond-center H in Si, $H_{BC}^{(+)}$, at 1998 cm^{-1} was measured to be $T_1 = 7.8 \pm 0.2$ ps at 20 K. There are several good reasons for studying H_{BC}^{+}: It is the most fundamental H-related defect in Si, and plays a key role in the reactions of H with defects and impurities. Moreover, it has been studied in great detail experimentally[76,83–86] and theoretically[87] and is thus well characterized. Finally, $H_{BC}^{(+)}$ gives rise to an intense absorption line at 1998 cm^{-1} due to the excitation of the stretch mode, where the H vibrates parallel to the Si–H–Si bond axis (Fig. 6).[76,83,84] The large absorption cross section of this mode makes it ideal for transient bleaching experiments.

Experimental studies of point defects require low defect concentrations in order to reduce the effect of interactions between defects, an additional source of inhomogeneous broadening. For transient bleaching spectroscopy on hydrogen-related local modes in proton-implanted silicon, the practical maximum concentration is at 0.2 at. %. Implantation of higher concentrations results in a broad absorption feature in the Si–H stretch range rather than an increase in the intensity of the sharp absorption lines of hydrogen-related point defects.[88] Pump–probe studies typically require area densities (doses) of hydrogen of $\sim 1\times10^{17}$ cm^{-2}. In order to meet both requirements, the samples were implanted with ions at a series of 28 different energies in the range 1.0–1.8 MeV, yielding a uniform H concentration C_H of 1.7×10^2 ppm formed from ~15 μm to a depth of 47 μm. The samples were cooled to 80 K during implantation which was accomplished by implanting into a cryostat attached to the end of the accelerator beam line. After implantation the cryostat was detached from the beam line and moved to the spectroscopic setup.

The vibrational lifetime of the 1998 cm^{-1} mode was measured using a standard pump–probe setup (Fig. 1). For experimental details see Ref. 82. Figure 7 shows the transient bleaching signal S_b as a function of time delay between pump and probe measured at ~20 K with the FEL. The data are well represented by a single-exponential decay with a time constant $T_1 = 7.8 \pm 0.2$ ps.

The excited 1998 cm^{-1} mode can in principle decay into photons, electronic degrees of freedom, or other vibrational modes. The radiative lifetime can be estimated to be of the order of milliseconds,[89] which rules out radiative decay as the dominating mechanism. Electronic decay can also be ruled out because the positive charge state of H_{BC} has no occupied electronic levels in the band gap. Consequently, only electronic transitions from the valence band to the conduction band or directly to the donor level of H_{BC} are possible, both of which require more energy than the 1998 cm^{-1} available. Budde and co-workers, therefore, concluded that the 1998 cm^{-1} mode decays into vibrational modes of the system consisting of a Si lattice with a H atom located at a bond-center site.[82]

The lifetime of the 1998 cm^{-1} mode has also been studied in the frequency domain by IRAS.[82] The shape of an absorption line is generally given by the convolution of its homogeneous line shape with a function describing the inhomogeneous broadening.[75] At very low temperatures the homogeneous line shape is Lorentzian with a FWHM (in cm^{-1}) given by

Downloaded 24 May 2004 to 129.59.117.76. Redistribution subject to AIP license or copyright, see http://jap.aip.org/jap/copyright.jsp

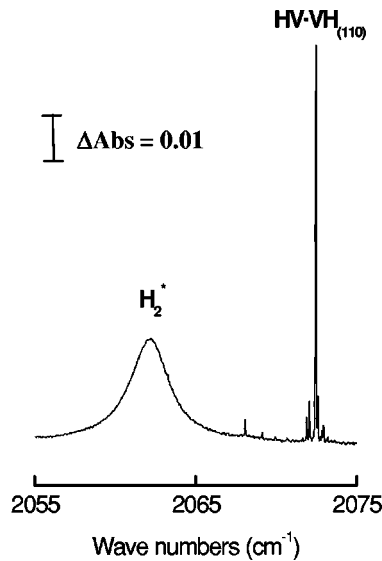

FIG. 8. IR absorbance spectrum of *e*-irradiated, H-doped Si, showing the lines of H_2^* and $HV\cdot VH_{(110)}$.

$$\Gamma_0=\frac{1}{2\pi c T_1}. \tag{44}$$

For LVMs in crystals, the inhomogeneous broadening is determined by the strain fields induced by lattice defects present in the sample. Since the most abundant imperfections in the H-implanted Si samples are defects formed during implantation, one would expect the inhomogeneous broadening to decrease with decreasing C_H.

Figure 6(a) shows the absorption line associated with the fundamental transition of the 1998 cm^{-1} mode measured with IRAS at ~10 K, which is well represented by a Lorentzian. The FWHM of the absorption line is shown in Fig. 6(b) as a function of C_H. The width decreases monotonically with decreasing C_H and nearly coincides with the natural linewidth obtained from Eq. (44) for C_H~1 ppm. Thus, the results obtained in time and frequency domains are fully consistent. Moreover, the convergence demonstrates that good estimates of the vibrational lifetime at low temperature can be obtained from IRAS on samples with low concentrations of H and lattice defects.

TABLE I. Lifetime T_1 for a selection of stretch modes of H-related defects in crystalline Si measured at ~10 K.

Defect	ω (cm^{-1})	T_1 (ps)	Ref.
H_2^*	2062	4.2	96
IH_2	1987	12	94
IH_2	1990	11	94
$H_{BC}^{(+)}$	1998	7.8	82
VH_2	2122	60	94
VH_2	2145	42	94
VH_4	2223	56	94
$HV\cdot VH_{(110)}$	2072	295	94

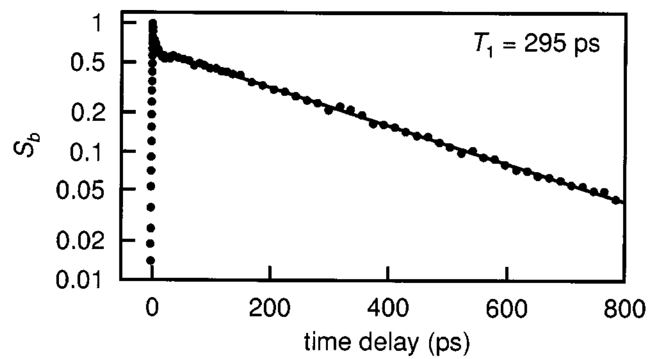

FIG. 9. Decay of the transient bleaching signal from the 2072.5 cm^{-1} mode of $HV\cdot VH_{(110)}$ at 10 K.

B. Structural dependence

When Si implanted with protons at cryogenic temperatures is heated above ~180 K, the 1998 cm^{-1} line disappears and a series of new lines is formed in the range 1800–2250 cm^{-1} (Fig. 4), which have been identified as Si–H stretch modes of distinct H-related defects (see e.g. Refs. 90–93). The average absorption cross section of these modes is ~25 times smaller than that of the 1998 cm^{-1} mode,[84] which makes direct lifetime measurements on these defects by transient bleaching spectroscopy much more difficult. However, one can estimate the lifetimes of these modes from their spectral widths at low temperature. As discussed in Sec. III,[82] the lifetime of the state $|1\rangle$ of a local vibrational mode is given by

$$T_1=\frac{1}{2\pi c\Gamma_0}, \tag{45}$$

where c is the speed of light and Γ_0 is the full width at half maximum of the absorption line, given in cm^{-1}, associated with the fundamental transition of the mode. For Eq. (45) to be valid, Γ_0 has to correspond to the natural linewidth, and measured FWHMs may have to be corrected for instrumental and inhomogeneous broadening.

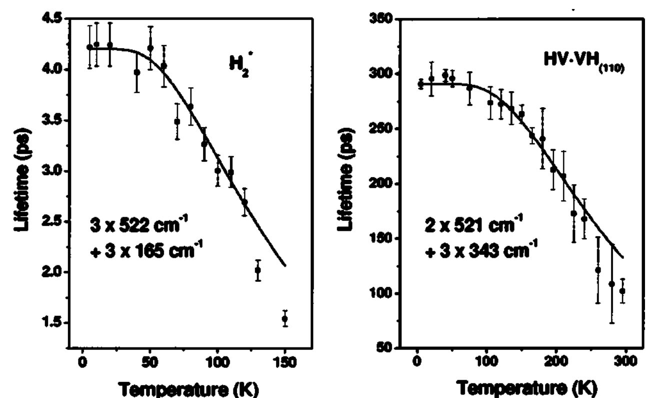

FIG. 10. Temperature dependence of T_1 of the 2062 cm^{-1} mode of H_2^* (left side) and the 2072 cm^{-1} mode of $HV\cdot VH_{(110)}$ (right side). The solid lines are fits from Eqs. (17) and (18) for decays into the sets of accepting modes {165, 165, 165, 522, 522, 522} cm^{-1} and {343, 343, 343, 521, 521} cm^{-1} of the 2062 and 2072 cm^{-1} modes.

Downloaded 24 May 2004 to 129.59.117.76. Redistribution subject to AIP license or copyright, see http://jap.aip.org/jap/copyright.jsp

To minimize the error in T_1 introduced by such corrections, Budde and co-workers performed IRAS measurements at the highest resolution possible using samples with very low defect concentrations.[94] The samples were 15 mm thick and consisted of n-type Si ($[\mathrm{As}]=3\times10^{14}\ \mathrm{cm}^{-1}$) grown by the float-zone method. As described in detail in Ref. 94, the samples were doped with H (Si:H) by annealing at 1250 °C for 30 min in quartz ampules containing H_2 gas at 0.66 atm. The concentration of H was $\sim1\times10^{16}\ \mathrm{cm}^{-1}$.[94] The point defects studied were created by irradiating the samples with 2.5 MeV electrons at RT to a total dose of $10^{17}\ \mathrm{cm}^{-2}$. Budde and co-workers estimated the defect concentration to be $\sim10^{16}\ \mathrm{cm}^{-3}$,[94] ~50 times smaller than in the proton-implanted samples studied in Ref. 82, which results in significantly less inhomogeneous broadening.

The IR absorbance spectra of the Si:H samples revealed a series of absorption lines in the Si–H stretch regions, some of which are shown in Fig. 8. The lifetimes of the Si–H modes were obtained in the following way: First, the FWHMs of the lines were obtained by fitting Lorentzian line shapes to the measured absorbance profiles. These FWHMs were then corrected for instrumental broadening, and the result was entered into Eq. (45). As shown in Table I, the lifetimes of Si–H stretch modes are extremely dependent on the defect structure, ranging from 4.2 ps for H_2^* to more than 295 ps for $HV\cdot VH_{(110)}$.[94] The narrowest line in the Si:H spectrum originates from the 2072.5 cm^{-1} mode of $HV\cdot VH_{(110)}$.[94,95] Having a width of only 0.0203 cm^{-1}, this mode has a lifetime of at least 262 ps. To obtain a reliable T_1 for this defect, Budde and co-workers measured the lifetime directly with transient bleaching spectroscopy. Figure 9 shows a semilog plot of the transient bleaching signal S_b versus time delay measured at ~10 K with the TJNAF FEL. The signal decreases exponentially with a time constant $T_1=295\pm6$ ps.[94]

Table I shows that the lifetimes of Si–H stretch modes depend strongly on the bonding configuration of the defects. For instance, the interstitial-type defects H_2^*, IH_2, and $H_{BC}^{(+)}$ have lifetimes of 4.2–12 ps, whereas the lifetimes of vacancy–hydrogen complexes are at least 40–295 ps. The most striking example of the structural dependence is the two orders of magnitude difference in the lifetime of the 2062 and 2072 cm^{-1} modes of H_2^* and $HV\cdot VH_{(110)}$. The strong structural dependence might be explained by either pseudolocalized modes or LVMs being involved in the decay process. Being localized around the defect, such modes have much larger vibrational amplitudes on the atoms close to the Si–H bond than, e.g., lattice phonons, which may cause a strongly enhanced anharmonic coupling to the Si–H stretch mode. However, significant distortions of the Si–Si bonds in the vicinity of the defects are required for pseudolocalized modes or LVMs to form,[17] which is consistent with highly distorted interstitial-type defects having shorter lifetimes than vacancy-type defects. Furthermore, to explain the large difference in lifetimes, one should also consider the anharmonic coupling strength between the stretch mode and the low-frequency modes. In the $HV\cdot VH_{(110)}$ center, it certainly seems plausible that the relatively large open volume of the vacancies would lead to a small interaction between the hydrogen and the surrounding silicon atoms. This small interaction would lead to a longer vibrational lifetime.

TABLE II. Lifetime T_1 for a selection of stretch modes of D-related defects in crystalline Si measured at ~10 K (Ref. 95).

Defect	Si-D ω (cm^{-1})	Si-D T_1 (ps)	Si-H T_1 (ps)
D_2^*	1500.1	4.8	4.2
ID_2	1446.5	20	12
ID_2	1448.7	18	11
VD_2	1547.9	70	60
VD_2	1565.1	55	42
VD_4	1617.5	143	56
$DV\cdot VD_{(110)}$	1510.4	93	295

C. Decay channels

Lüpke and co-workers investigated the vibrational relaxation channels of the 2062 and 2072 cm^{-1} modes of H_2^* and $HV\cdot VH_{(110)}$ in Si, in order to elucidate the two-orders-of-magnitude difference in their lifetimes.[96] The lifetime T_1 of these modes is measured as a function of temperature by time-resolved transient bleaching spectroscopy. Figure 10 shows T_1 versus temperature for H_2^* (left side) and $HV\cdot VH_{(110)}$ (right side). In the case of the 2062 cm^{-1} mode, T_1 is nearly constant up to ~60 K, where it starts to decrease, reaching half of its low-temperature value at 130 K. The solid lines in Fig. 10 are fits using Eq. (17) with the vibrational relaxation channel of the 2062 cm^{-1} mode represented by a set of six accepting modes {165, 165, 165, 522, 522, 522} cm^{-1}. This set of accepting modes is very similar to that of the 1998 cm^{-1} mode of bond-center H in Si,[82] which is well described by decays into six accepting modes, {150, 150, 150, 516, 516, 516} cm^{-1}. In contrast, the lifetime of the 2072 cm^{-1} mode starts to decrease at ~120 K reaching half of its low-temperature value at 250 K. The decay channel of the 2072 cm^{-1} mode is well represented by five accepting modes with frequencies {343, 343, 343, 521, 521} cm^{-1}.

The vibrational relaxation channels are not uniquely determined by the temperature dependence of the lifetimes. In particular, the high-frequency phonon modes of the decay channels do not have a strong influence on the temperature dependence of the lifetimes. For example, the temperature dependence of the 2072 cm^{-1} mode is equally well represented by a set of accepting modes of {343, 343, 343, 343, 700} cm^{-1}. However, the wave number of the accepting mode with the lowest frequency is quite well determined by the onset of the temperature dependence of T_1, for example, ~60 K for H_2^* and ~120 K for $HV\cdot VH_{(110)}$. Figure 10 also shows that in both cases the calculations using Eq. (17) deviate from the measured T_1 at elevated temperatures, indicating that additional relaxation channels may increase the decay rate at higher temperatures. The low-frequency accepting modes of 165 cm^{-1} for H_2^* (and 150 cm^{-1} for bond-center hydrogen) nearly coincide with transverse acoustic (TA) phonons of the undistorted Si crystal, which have been calculated in Ref. 97. Likewise, the 343 cm^{-1} modes involved

Downloaded 24 May 2004 to 129.59.117.76. Redistribution subject to AIP license or copyright, see http://jap.aip.org/jap/copyright.jsp

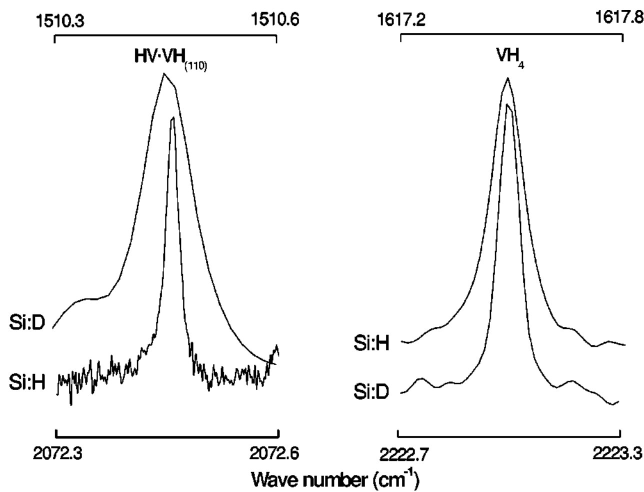

FIG. 11. Comparison of the Si–H (full) and Si–D (dashed) absorption lines of $HV\cdot VH_{(110)}$ and VH_4.

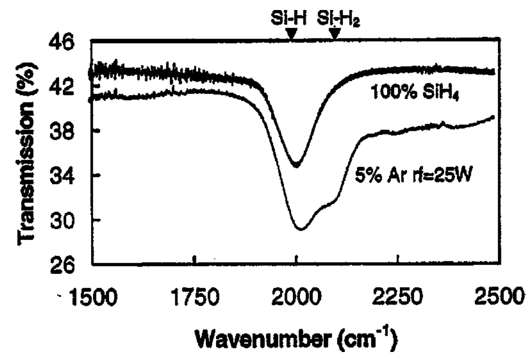

FIG. 12. FTIR spectra of *a*-Si:H showing the Si–H and Si–H_2 stretch bands at 2000 and 2090 cm^{-1} (with permission from Ref. 111).

in the decay of the stretch mode of $HV\cdot VH_{(110)}$ nearly coincide with the peak in the longitudinal acoustic (LA) phonon density.

The fact that these modes have very different lifetimes is surprising at first glance considering that both Si–H stretch modes have nearly the same frequency and symmetry, and the compound density of accepting phonon states of the unperturbed lattice $\rho_{\{\nu\}}$ is almost identical. The critical difference between these defects is their local structure, interstitial or vacancy like, which gives rise to a very different local vibrational mode structures, referred to as pseudolocalized modes (PLMs). Evidently it is these local modes that govern the lifetimes, and are responsible for the observed preferential couplings to characteristic bulk phonons. A more detailed understanding of the nature of these PLMs is required to fully elucidate the vibrational energy relaxation and transfer channels in solids.

D. Deuterium lifetimes

Lyding, Hess, and Kizilyalli demonstrated that H plays an active role in the degradation process of silicon metal–oxide–semiconductor field-effect transistors (MOSFETs) by showing that devices treated with deuterium (D) have transconductance lifetimes 10–50 times longer than H-passivated devices.[98] Similar "giant isotope effects" have been observed in other contexts.[21,99,100] Dissociation of Si–H and Si–D bonds is believed to be caused by inelastic electron scattering, which excites the bond to either a dissociative electronic state or to excited vibrational states.[21–24]

The vibrational excitation mechanism of hydrogen-related modes has been described by the truncated harmonic oscillator (THO) model.[21–24] This model describes the Si–H and Si–D bonds as harmonic oscillators, and assumes that the bonds dissociate at a rate given by the rate of excitation from the highest bound vibrational state $|N_{max}\rangle$ to the lowest unbound state $|N_{max}+1\rangle$. Within this model, the dissociation rate is approximately given by

$$R\sim\frac{N_{max}+1}{T_1}\left(\frac{\Gamma_{exc}}{\Gamma_{exc}+1/T_1}\right)^{N_{max}+1}, \qquad (46)$$

where T_1 is the lifetime of the vibrational state $|1\rangle$ and Γ_{exc} is the excitation rate of the $|0\rangle\rightarrow|1\rangle$ transition.[21–24] The THO model is in qualitative agreement with H desorption experiments.[23,24] However, this agreement may be fortuitous: For instance, it is well known that Si–H and Si–D bonds are anharmonic, which causes the level spacing to decrease with increasing *N*. This will affect the value of N_{max} in Eq. (46), and hence, also the desorption rate predicted by the model. Moreover, the assumption of a single normal mode may not be justified, since both the stretching and the bending modes may play a role in the dissociation process.[25] Despite these potentially unjustified assumptions, the THO model provides a framework for discussing bond dissociation via vibrational excitation. For instance, it is evident from Eq. (46) that Γ_{exc} has to be on the order of the decay rate, $1/T_1$, for bond breaking to proceed via this mechanism. The model also provides a simple explanation for the H/D isotope effect. For instance, N_{max} for Si–D is $\sim\sqrt{2}$ times greater than for Si–H, which would lead to a great reduction in the dissociation rate. Moreover, Si–D modes are usually believed to have shorter T_1 than the corresponding Si–H modes,[25] which would make the isotope effect even greater.

Table II shows the lifetimes of the Si–D stretch modes, and allows for a direct comparison of the lifetimes of H-and

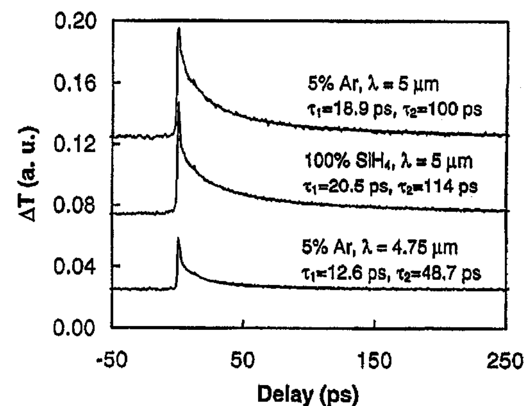

FIG. 13. Decay of the transient bleaching signal from the Si–H and Si–H_2 stretch modes in *a*-Si:H (with permission from Ref. 111).

Downloaded 24 May 2004 to 129.59.117.76. Redistribution subject to AIP license or copyright, see http://jap.aip.org/jap/copyright.jsp

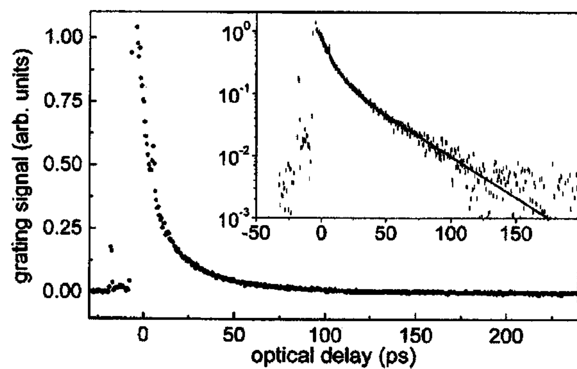

FIG. 14. Transient-grating signal from the 2000 cm^{-1} stretch band of *a*-Si:H taken at room temperature (with permission from Ref. 112).

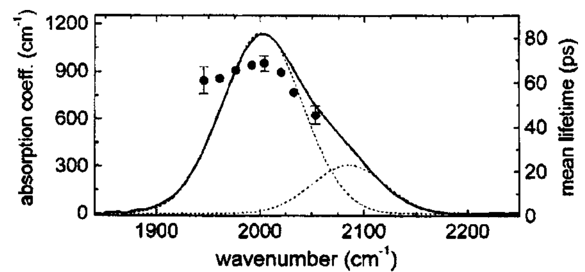

FIG. 15. Spectral dependence of the geometric mean lifetime (circles) at 10 K. The linear absorption spectrum (solid line) is shown along with the contributions from mono- and polyhydride (dashed lines) (with permission from Ref. 112).

D-related LVMs. Substitution of H with D affects the lifetime of LVMs in two ways. First, the vibrational amplitude is less for Si–D modes than for Si–H modes, and since the decay of the LVM into other modes is an anharmonic effect, Si–D modes have longer lifetimes than the corresponding Si–H modes. Second, the vibrational energy of the Si–D mode is $\sim\sqrt{2}$ less than that of the Si–H mode. Consequently, the order of the decay process, i.e., the number of modes into which the LVM decays, can be smaller for Si–D than for Si–H. Since the strengths of anharmonic terms are expected to decrease with increasing order, this suggests that Si–D modes have shorter lifetimes than the corresponding Si–H modes. Until recently, the second contribution has been assumed to be dominant,[25] which is consistent with the experimental results for Si–H and Si–D modes on H-terminated Si surfaces.[101] In contrast, Table II shows that the lifetimes of D-related stretch modes are longer than the corresponding Si–H lifetimes for all defects except $HV\cdot VH_{(110)}$, for which the Si–D lifetime is three times shorter than for Si–H. Figure 11 shows the inverted isotope effect for $HV\cdot VH_{(110)}$. According to Eq. (46), the inverted isotope dependence of T_1 observed for $HV\cdot VH_{(110)}$, implies that this defect, and perhaps also P_b:H centers at the Si/SiO_2 interface, exhibits much larger differences in Si–D and Si–H dissociation rates than most other H-related defects.

No H-related centers at the Si/SiO_2 interface, including P_b:H, have ever been observed directly. It is, therefore, quite likely that the giant isotope effect will have to be explained by theoretical methods. The lifetime data provide an indispensable benchmark for such theory.

V. AMORPHOUS SILICON

In hydrogenated amorphous silicon (*a*-Si:H), the presence of hydrogen eliminates most of the defects. As a result, high-quality *a*-Si:H layers can be grown. However, the introduction of excess carriers through moderate illumination or electronic injection increases the density of dangling bonds (DBs) to nearly 10^{17} cm^{-3}, even in the most degradation resistant materials.[102–106] These excess carrier-induced DBs are metastable; they are annealed out in a few hours at about 150 °C. However, their rapid formation sharply limits application of *a*-Si:H as an inexpensive material for photovoltaic and electronic applications. The source of the carrier-induced metastability has been elusve; since its discovery by Staebler and Wronski (SW) in 1976,[107] several models have been published, but no previous model is satisfactory.[108,109] Branz recently proposed a hydrogen collision model to explain the SW effect.[110] In this model, DBs are created when recombination of light-induced carriers stimulates emission of mobile H from Si–H bonds to form a mobile Si–H–Si bond-centered H configuration leaving a DB behind. A collision of two mobile H atoms creates a metastable complex containing a pair of Si–H bonds in close proximity. The two mobile H are then immobilized. Light-induced or thermal annealing of the SW effect leads to the breakup of the metastable complex and the subsequent retrapping of the mobile H to DBs completes the SW annealing. A detailed knowledge of the rates and pathways of vibrational energy flow from the Si–H bonds may provide some information about the degradation mechanism of *a*-Si:H.

A. Hydrogen stretch band

Xu and co-workers reported the first direct measurement of the vibrational lifetime of the Si–H and Si–H_2 stretching modes in *a*-Si:H obtained by the equal-wavelength pump–probe technique using the stanford FEL.[111] Figure 12 shows the Fourier transform infrared (FTIR) spectrum of the *a*-Si:H films grown at low substrate temperature (250 °C) on (100) *c*-Si wafers to eliminate most defects. The band at 2000 cm^{-1} is due to the Si–H stretching mode and the band at

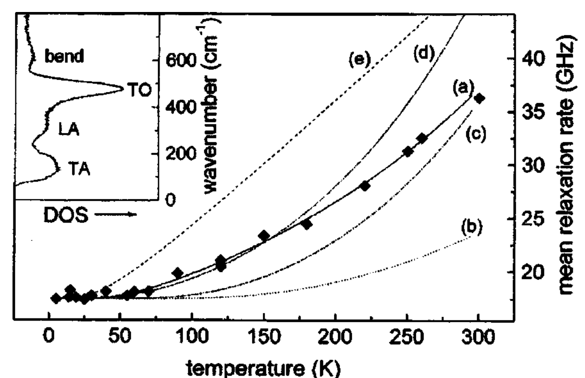

FIG. 16. Temperature dependence of the mean decay rate (inverse lifetime). Also indicated are various possible decay channels (a)–(e). The phonon density of *a*-Si:H is shown in the inset (with permission from Ref. 113).

Downloaded 24 May 2004 to 129.59.117.76. Redistribution subject to AIP license or copyright, see http://jap.aip.org/jap/copyright.jsp

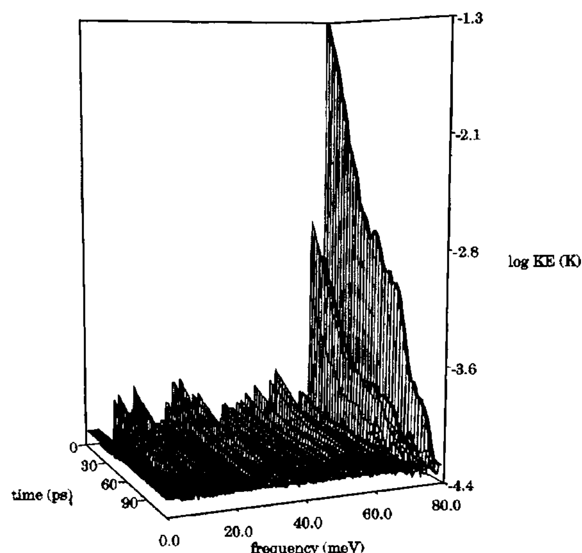

FIG. 17. Average kinetic energy as a function of time and frequency after excitation of the 78.7 meV mode (with permission from Ref. 115).

2090 cm^{-1} to the Si–H_2 stretching mode. All of the peaks have a full width at half maximum of ~100 cm^{-1}.

Figure 13 shows the decay of the transient bleaching signal for the two wavelengths, 5.0 and 4.75 μm, in resonance with the Si–H and Si–H_2 stretching mode, respectively.[111] The data can be fitted very well with a biexponential function using the following expression:

$$\Delta T \propto A_1 e^{-\tau/\tau_1} + A_2 e^{-\tau/\tau_2}, \quad (47)$$

where τ_1 and τ_2 ($\tau_1 < \tau_2$) are two relaxation times. The energy relaxation times of the Si–H stretch mode are ~20 and ~100 ps for both samples whereas the energy relaxation times of the Si–H_2 stretch mode are ~13 and ~50 ps.[111] Xu and co-workers proposed a model in which each time constant corresponds to a different physical process in the material.[111] In this model, the faster decay time corresponds to redistribution within the Si–H stretch vibrational band, and the slower time to energy transfer from the stretch mode to low-frequency accepting modes.

Rella and co-workers reported pump–probe and transient-grating lifetime measurements performed on the Si–H stretch mode as a function of temperature and wavelength using the FELIX laser.[112,113] From these data the authors concluded that energy redistribution does not occur to a significant extent within the Si–H stretch vibrational band, and that the stretch mode decays primarily into three bend quanta plus one TA-like bulk phonon. Therefore, the stretch vibrations are localized, and do not form a phonon-like band of states.

Rella and co-workers performed primarily transient-grating experiments, which permits lifetime measurements with extremely high signal-to-noise ratio, since the diffracted signal is detected against "zero" background.[112,113] Figure 14 shows a typical scan taken at room temperature, showing the decay of the transient-grating signal.[112] The data are fit to the square of a double exponential, and decay times of 10.6 and 74.5 ps were obtained, which are in agreement with the relaxation times obtained from transient bleaching by Xu *et al.*[111]

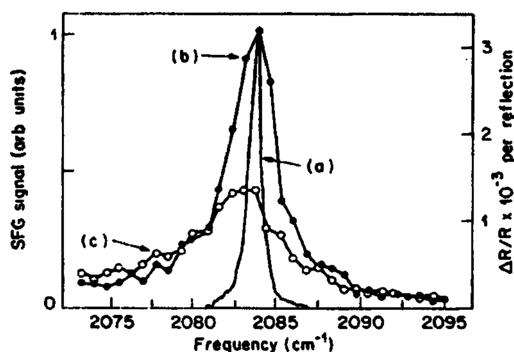

FIG. 18. Si–H spectra from the Si(111):H surface: (a) linear absorption, (b) SFG, and (c) SFG after transient bleaching (with permission from Ref. 101).

Rella and co-workers performed also lifetime measurements as a function of temperature, and across the Si–H monohydride absorption band.[112] Because the shape of the measured decay curves remained unchanged, it is possible to define a geometric mean lifetime $\sqrt{\tau_{\rm fast}\tau_{\rm slow}}$ of the Si–H stretch mode shown in Fig. 15 for a temperature of 10 K.[112] Since the wavelength dependence of the lifetime does not change with temperature the authors conclude that the stretch mode does not form a vibrational band in *a*-Si:H.

Figure 16 shows the mean lifetime as a function of temperature.[113] It is clear that only the decay channel of three bending modes plus one TA phonon fits the data well. Therefore, even after the decay of the stretch mode, the vibrational energy remains largely localized in the form of bend mode excitation, with only a small fraction of the energy dissipating into the phonon bath of the amorphous-Si host. The reason for the strongly nonexponential decay of the vibrational lifetime is still unclear. It is likely that disorder in the material leads to a wide variation in the microscopic environment of the hydrogen, thus leading to a wide distribution of vibrational lifetimes as well as the observed broadening of the absorption line. Such a view is qualitatively consistent with the single-crystal data where large variations in lifetime are associated with minor changes in defect configurations. Investigations are currently underway to test this model, as well as to examine the possibility of applying these techniques to a variety of problems, ranging from a detailed study of the effects of visible light aging on the structure of amorphous silicon, to a more fundamental inquiry into the nature of disordered materials.

B. Molecular dynamics simulations

Fabian and Allen[114] and Bickham and Feldman[115] calculated vibrational lifetimes in amorphous silicon. Both groups used the same potential and structural models in their study except that the later group also made use of a 4096 atom model in addition to a 216 atom model. Phenomenological structural and interatomic potential models were employed. Both groups found that at moderate temperatures, lifetimes are on the order of 10 ps and lifetimes of localized and ex-

Downloaded 24 May 2004 to 129.59.117.76. Redistribution subject to AIP license or copyright, see http://jap.aip.org/jap/copyright.jsp

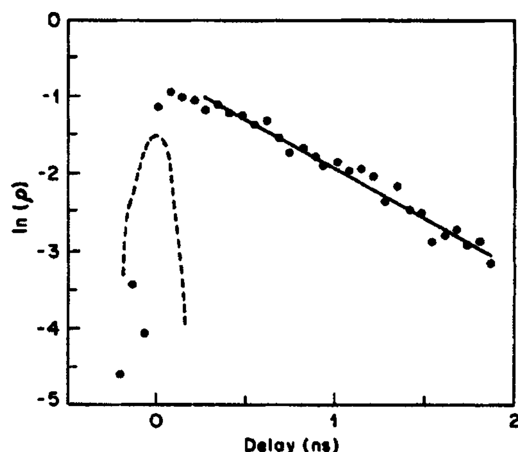

FIG. 19. Decay of the transient bleaching signal from the Si–H stretch mode on the Si(111):H surface. The solid line is a least-squares fit giving $T_1=795$ ps. The dashed curve indicates the temporal resolution (with permission from Ref. 101).

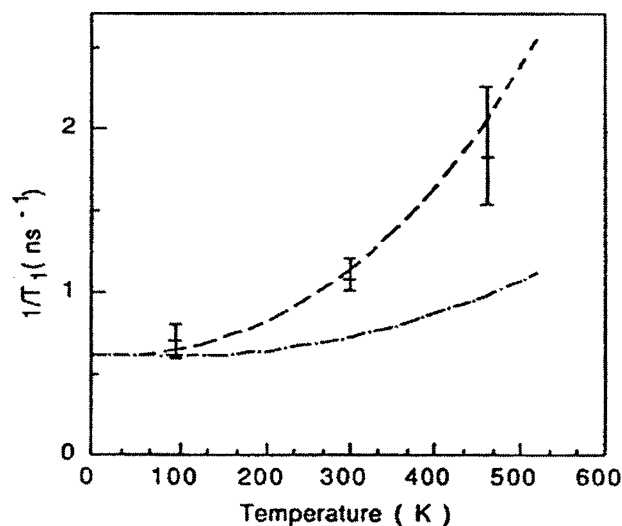

FIG. 20. Temperature dependence of the lifetime of the Si–H stretch mode on Si(111):H surface (with permission from Ref. 101).

tended nonpropagating modes are comparable. Bickham and Feldman calculated the vibrational lifetimes for models of amorphous silicon using molecular dynamics simulations.[115] These types of numerical experiments have been used increasingly to study the properties of amorphous materials. They have been used to investigate the Raman spectrum of amorphous silicon[116] and high-frequency modes in fused silica.[117] Although the use of atomistic models restricts the interpretation to the classical regime, experimentally relevant information about the amorphous structure and vibrational modes has been obtained.

In these computer simulations, the instantaneous displacements, velocities, and accelerations are used as initial conditions. The kinetic energy is introduced into selected modes of vibration and monitored as a function of time. Figure 17 shows the log kinetic energies of all 648 modes of a 216 atom supercell as a function of time and frequency for an initial excitation of the highest-frequency mode with $\omega_0=78.7$ meV. Although the excitation energy is put into a single mode, a small portion is quickly and nonradiatively transferred to other modes by anharmonic coupling. The initial kinetic energy spectrum, therefore, has a strong peak at the perturbation frequency with secondary peaks at lower frequencies. As the simulation progresses, this nonequilibrium distribution evolves into a microcanonical ensemble with each mode having the same kinetic energy. The time scale for this relaxation is on the order of tens of picoseconds, and similar decay times have been obtained for other localized and extended, nonpropagating modes in the 216 atom model.[118]

These MD simulations using large amorphous supercells demonstrate the ability to extract experimentally relevant information from computer simulations. The lifetimes found by this method are in good agreement with the perturbative calculations of Fabian and Allen[114] and are on the order of 10 ps at low temperatures in both 216 and 4096 atom supercells. The lifetimes of high-frequency localized modes and extended, nonpropagating modes with intermediate frequencies are comparable. Although these initial calculations of the vibrational lifetimes in amorphous silicon did not include the Si–H stretch vibration, the obtained decay rates of the high-frequency localized modes are comparable. Future MD simulations on hydrogenated amorphous silicon can be used to elucidate the strongly nonexponential decay of the Si–H stretch mode.

VI. SILICON SURFACES

The first studies on the relaxation dynamics of adsorbate vibrations used conventional linear absorption and transient bleaching. To compensate for the weak surface optical density, poorly characterized high surface area materials had to be used.[119–121] On the other hand, to study single-crystal surfaces, the potential of the nonlinear optical techniques of sum–frequency generation was recognized early.[71–74,122]

Since then, data on the relaxation of adsorbates on single-crystal metal,[123,124] semiconductors,[101] and insulator surfaces[125] have been available using SFG transient reflectivity or fluorescence techniques. This section surveys the pioneering work done by Guyot-Sionnest and co-workers on the lifetime of the Si–H stretching vibration for the Si(111)/H:1×1 and Si(100)/H:2×1 surfaces. Theoretical results have been obtained by a method that combines Bloch–Redfield theory with MD simulations (Sec. VI C).

A. Si(111):H surface

Guyot-Sionnest, Dumas, Chabal, and Higashi presented the first time-resolved measurements of the vibrational lifetime of the Si–H stretch mode for an ideally H-terminated Si(111) surface.[101] The hydrogenated surface is characterized by a single Si–H stretch vibration at 2083.7 cm^{-1} polarized purely perpendicularly to the surface (Fig. 18). Furthermore, in contrast to the many relaxation channels available to molecules on metals (electronic, intramolecular) with strong dynamic dipoles (intermolecular), the Si–H stretch mode can only relax via anharmonic coupling to one H mode (Si–H bend) or to the substrate motion (Si surface phonons). The absence of resonant electronic excitation and the large en-

Downloaded 24 May 2004 to 129.59.117.76. Redistribution subject to AIP license or copyright, see http://jap.aip.org/jap/copyright.jsp

ergy difference between the Si–H stretch mode and the other vibrational modes [$\nu_{\text{Si-H,bend}}=637\ \text{cm}^{-1}$ (Ref. 126) and $\nu_{\text{phonon}}\leqslant 500\ \text{cm}^{-1}$] imply that a long lifetime is expected. The temperature dependence of the Si–H stretch linewidth implies, in fact, that this mode is anharmonically coupled to both the Si–H bend and a Si surface phonon at a lower frequency, leading to a well-defined (dephasing or T_2) broadening.[127] Furthermore, molecular-dynamics calculations with no adjustable parameters (i.e., based on *ab initio* calculations) have been performed for this system.[128]

To measure the lifetime of the Si–H stretch on the Si(111) surface, Guyot-Sionnest and co-workers used the method of transient bleaching in conjunction with the surface-specific SFG technique.[101] In this scheme (Sec. III C) an intense infrared pulse resonant with the Si–H stretch vibration at 2083.7 cm^{-1} pumps the ground state into the first excited state. After a varying delay, the difference between the population of the ground state and the excited vibrational state $\Delta\rho$ is then probed by SFG from a pair of weaker infrared and visible beams. If the nonresonant contribution is small and the anharmonicity is larger than the bandwidth of the laser pulse, then the SFG signal is just proportional to the square of $\Delta\rho$. Therefore, as for the transient bleaching, one measures a ground-state recovery time.

Although the infrared cross section is small, the SFG signal is fairly strong because of a significant Raman cross section and the perfect ordering of the surface (Fig. 18). Figure 18(c) shows the SFG spectrum obtained with the pump coming 200 ps before the probe beam. The saturation of the absorption leads to a 60% decrease of the SFG signal. The ground-state recovery time is then directly obtained by varying the delay between the pump and probe and measuring the remaining saturation. The data are presented as the ratio $\rho \equiv 1-r^{1/2}\approx 2\rho_{\text{exc}}$ in Fig. 19 where $\ln(\rho)$ is plotted versus time delay. Within the experimental accuracy a straight line is observed with a lifetime $T_1=0.8\pm 0.1$ ns of the Si–H stretch vibration.

This lifetime is very long compared to what one would assume for chemisorbed molecules on surfaces. It illustrates the fact that the Si–H stretching mode is well decoupled from the bending mode and the substrate phonons. In addition, unlike molecules on metals, transfer to electronic excitations cannot occur since the band-gap energy is much larger than the vibrational quantum. The lifetime as a function of temperature is shown in Fig. 20.[101] The temperature dependence of T_1 is well represented by a decay mechanism involving three bending modes around 630 cm^{-1} and one silicon phonon around 200 cm^{-1} (dashed curve in Fig. 20). This decay channel was confirmed by theoretical calculations using perturbation theory by Gai and Voth[132] (Sec. VI C).

The work by Guyot-Sionnest and co-workers constitutes measurements of the lifetime of an adsorbate–substrate vibration. The system, ideal in many aspects, gives a clear, single-exponential decay of a spectrally well-defined vibrational mode. This measurement, along with the thorough linewidth study,[127] gives a complete experimental characterization of the anharmonic coupling between the Si–H stretch and the lower-frequency modes. This long Si–H stretch lifetime may allow various surface photophysics experiments to be done, such as multiphoton absorption, selective desorption, and chemical reaction.

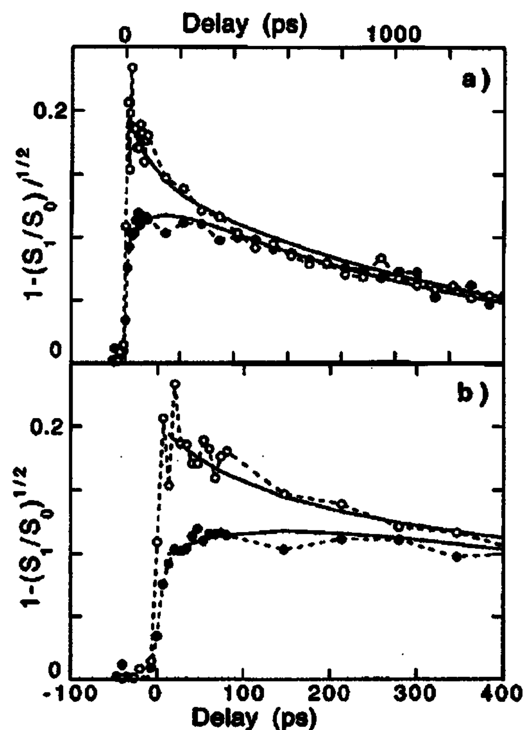

FIG. 21. Decay of the *S* mode on Si(100):H surface at 100 K with the pump resonant with the *S* (open circles) and *A* modes (closed circles) (with permission from Ref. 129).

B. Si(100):H surface

For Si(100)/H:2×1 the lifetime, from classical molecular dynamics, was predicted to be in excess of 20 ns,[126] much longer than the lifetime on Si(111)/H:1×1. Overall, the picture looks *a priori* fairly different for both surfaces. The measured lifetimes at low temperatures are highly sensitive to the sample preparation and thus reflect more the influence of defects than an intrinsic relaxation rate. Lifetimes longer than 6 ns have been observed at 100 K.[129] Si(100)/D:2×1 shows a shorter lifetime (250 ps) and much higher

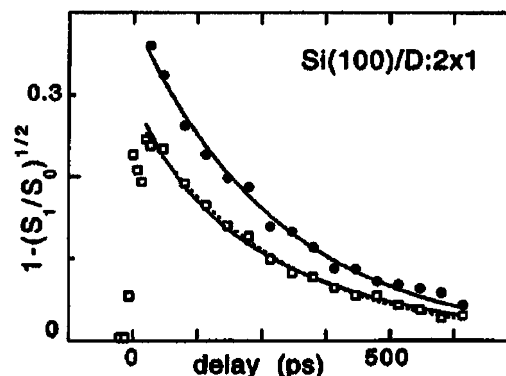

FIG. 22. Decay of the transient bleaching signal from the Si–D stretch mode on the Si(100):D surface at 300 K (full circles) and 100 K (open squares). The solid lines are single-exponential fits giving $T_1=225$ ps at 300 K and $T_1=218$ ps at 100 K (with permission from Ref. 129).

Downloaded 24 May 2004 to 129.59.117.76. Redistribution subject to AIP license or copyright, see http://jap.aip.org/jap/copyright.jsp

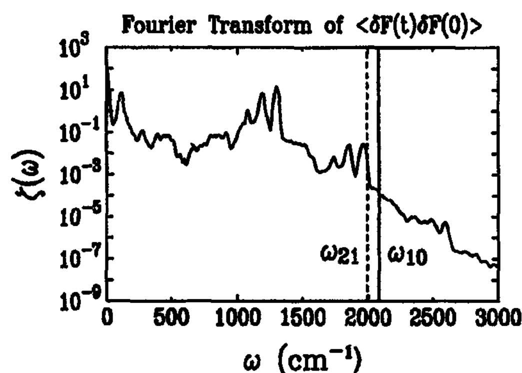

FIG. 23. Fluctuating force autocorrelation function along the Si–H bond at 300 K (with permission from Ref. 132).

reproducibility.[129] Guyot-Sionnest and co-workers have observed the energy transfer between the symmetric and antisymmetric modes of the surface dimers at low temperature.[129]

For the Si(100)/H:2×1 surface the coupling of the two Si–H bonds in the unit cell induces a symmetric (S) 2099 cm^{-1} mode and an antisymmetric (A) 2087 cm^{-1} mode.[130] The A mode is relatively weak in the SFG response due to small effective $\chi^{(2)}$ components. For IR light polarized parallel (p-pol.) to the plane of incidence, the S mode is very dominant with no detectable A mode contribution. With the IR pulse $\approx$80% vertically polarized (s-pol.), the A mode dominates but it is about 30 times weaker.

To probe the population dynamics of the system, both modes were pumped and the S mode was probed.[129] Figure 21 shows saturation spectra obtained at 100 K with the pump 80% s-pol., where saturation of the S mode induced by pumping either modes appears clearly. Both response curves were fitted with a fast decay component $T_{1,AS}=90\pm15$ ps and a slow decay, $T_1=1.3\pm0.1$ ns.[129] Therefore, the energy transfer between both modes ($T_{1,AS}$) is relatively slow at 100 K. It is faster at higher temperatures and not noticeable at room temperature.

While the relaxation rate is fairly consistent at room temperature to 1.25 ± 0.1 ns, the low-temperature data showed consistently $T_{1,AS}=90$ ps but T_1 decreased from 8 to 1.2 ns in the course of several days and cooling cycles.[129] This strong dependence of T_1 on the sample history is an indication that T_1 is not the intrinsic lifetime but is due to defect-induced relaxation. A detailed study of several samples revealed that T_1 at 100 K can be longer than 6 ns while at 300 K it is around 1.2 ns.[129] This temperature dependence is much stronger than for Si(111) since there the relaxation varied from 0.9 to 1.4 ns in the same temperature range (Fig. 20). Such a temperature dependence cannot be explained by a multiphonon relaxation process unless very low-energy phonons are involved ($\sim$100 cm^{-1}). The defects responsible for the enhanced relaxation rate are not known.

Si(100)/D:2×1 also showed a strong SFG resonance from the S mode though at 1530 cm^{-1}. The relaxation occurs over 250 ps with little variation (30 ps) from sample to sample.[129] This appears to be the intrinsic value for the lifetime of the deuterium stretch mode. Measurements taken at 300 and 100 K also showed little difference (Fig. 22).[129] The faster relaxation of Si–D and its weak temperature dependence are consistent with a multiphonon relaxation process of lower order now probably involving three Si–Si phonons since the Si–D bending mode is below the Si phonon edge (520 cm^{-1}).[131] The reliability of the measurement on Si(100)/D:2×1 is attributed to the shorter intrinsic relaxation time that prevents defects from playing an important role.[129]

C. Theoretical results

Tully and co-workers performed the first theoretical study of the lifetime of the Si–H stretch vibration on a Si surface using a classical Langevin dynamics calculation.[128] These authors obtained an estimate for the lifetime of the $v=1$ Si–H vibrational level on a model Si(100) surface to be $T_1\geqslant2\times10^{-8}$ s, which is much larger than the experimentally observed lifetime of $T_1\simeq1.5\times10^{-9}$ s.[101] First attempts to treat this problem within perturbation theory were undertaken by Gai and Voth.[132] These authors calculated the vibrational relaxation rate of an excited Si–H stretch mode on the ideally H-terminated H/Si(111)1×1 surface using a method that combines Bloch–Redfield theory with classical MD simulations (see Sec. II A).[26–29] In the calculation by Gai and Voth,[132] it has been assumed that the Si–H vibrational energy relaxation dynamics can be understood by studying the quantum population evolution for only one of the Si–H oscillators on the H/Si(111)1×1 surface. This local-mode-like picture neglects the mobility of the vibrational excitations between the equivalent Si–H oscillators on the surface. The latter effect should be more relevant to the vibrational dephasing dynamics[23] than to the energy relaxation process (i.e., each of the equivalent Si–H oscillators should have an identical energy decay pathway into the bulk).

The Redfield equations [Eqs. (3)–(5)] were solved numerically for the four lowest-energy levels of the chosen Si–H oscillator.[132] From the slope of the logarithm of the $v=1$ state probability versus time, the theoretical lifetime of the $v=1$ state was determined to be 1.7 ± 0.1 ns.[132] The corresponding experimental value is 0.95 ns.[101] Gai and Voth considered also the dominant damping term in the reduced density matrix equation for the $v=1$ state probability, to elucidate the mechanism for the Si–H stretching relaxation.[132] The Fourier transform of the fluctuating force autocorrelation function shown in Fig. 23 provides useful information on the coupling between the Si–H stretch and the rest of the system. The fundamental transition frequency $\omega_{10}=2084\ cm^{-1}$ is shown by the solid vertical line in Fig. 23. This transition frequency is somewhat to the blue of a prominent feature in the transform of the force autocorrelation function, which can be attributed to the second overtone (i.e., three quanta) of the Si–Si–H bending motion ($\omega_{bend}\sim640\ cm^{-1}$). Gai and Voth suggested that the $v=1$ state relaxes through coupling to a combination state consisting of three Si–H bending quanta plus a phonon to make up the small frequency mismatch (as postulated in Refs. 101, 128, 133 and 134). This result was confirmed by Ermorshin and co-workers who used a quantum mechanical treatment of the highly localized

Downloaded 24 May 2004 to 129.59.117.76. Redistribution subject to AIP license or copyright, see http://jap.aip.org/jap/copyright.jsp

Si–H bending modes.[135] In the approach by Gai and Voth the bending modes are treated classically as bath modes.[132] An important result of the calculations by Gai and Voth is the fact that the coupling between the Si–H stretch and the Si–Si–H bends is kinetic in character.[132] For the simple potential energy function employed in these calculations, there are no potential energy coupling terms between the Si–H stretch and the Si–Si–H bends. This behavior has also been identified, e.g., in the study of vibrational energy relaxation in isolated molecules.[136]

It is also possible to calculate the lifetime of the $v=2$ state, which is thought to be considerably shorter than the lifetime of the $v=1$ state. The Fourier transform of the fluctuating force autocorrelation function at the frequency $\omega=\omega_{21}$ is shown by the vertical dashed line in Fig. 23. Clearly, the $v=2$ state of the Si–H stretch is more closely on resonance with the bending-mode-induced peak in Fig. 23. Correspondingly, the calculated lifetime is 0.13 ns, which is ~10 times shorter than that calculated for the $v=1$ fundamental. The level of agreement between theory and experiment is more uncertain in this case because the linewidth is dominated by dephasing broadening. More accurate calculations based on improved potential energy functions are the subject of future research.

VII. CONCLUSIONS AND OUTLOOK

Before closing, we would like to place the current experimental and theoretical accomplishments in this emerging field in the proper perspective. Budde and co-workers have measured the lifetimes of a selection of Si–H stretch modes of point defects in Si. The lifetimes of interstitial-type defects were found to be very short (1.6–8 ps), whereas vacancy-type defects have lifetimes up to several hundreds of picoseconds—two orders of magnitude variation. The strong dependence of the lifetime on the atomic structure of the defect suggests that pseudolocalized modes or LVMs are involved in the vibrational relaxation of Si–H bonds of point defects in solids. Moreover, to explain the large difference in lifetimes, one should also consider the anharmonic coupling strength between the stretch mode and the low-frequency modes. It certainly seems plausible that the relatively large open volume of the vacancies would lead to a small interaction between the hydrogen and the surrounding silicon atoms. This small interaction would lead to a longer vibrational lifetime. This interpretation is consistent with the observed long vibrational lifetime of hydrogen bonded to Si surfaces. Both the Si(111)/H and the Si(100)/H:2×1 systems have Si–H lifetimes in excess of 1000 ps at ~100 K,[101,129] i.e., 2–3 orders of magnitude longer than for Si–H stretch modes of interstitial-type point defects.

Furthermore, the measured vibrational lifetimes of the corresponding Si–D stretch modes are key to understanding the physics of the giant isotope effect. Against conventional wisdom, lifetimes of Si–D modes are found to be typically longer than for the corresponding Si–H modes. Hydrogen-terminated dangling bonds, exemplified by the $HV\cdot VH_{(110)}$ complex, have particularly long lifetimes, and the H/D isotope dependencies of their lifetimes are "inverted." The inverted isotope dependence is also found for H/D stretch modes on Si surfaces. Based on this observation, it is possible that P_bH: centers might be particularly susceptible to dissociation by multiple vibrational excitation, and are likely to exhibit a particularly large isotope effect. No H-related centers at the Si/SiO_2 interface, including P_b:H, have been observed directly. It is, therefore, quite likely that the giant isotope effect will have to be explained by theoretical methods.

Finally, it is interesting to compare the results by Budde and co-workers with measurements of Si–H modes in different environments. The lifetime of Si–H stretch modes in amorphous Si (a-Si:H) was studied by pump–probe and transient-grating spectroscopy. In this material, the population relaxation is biexponential with a short decay time of ~10 ps and a long decay time of ~100 ps.[111,112] The fast component was initially ascribed to redistribution within the Si–H stretch band and the slow component to decay of the Si–H stretch modes into Si–H bend modes or phonons.[111] However, more recent experiments indicate that the two decay times are due to stretching vibrations at different sites having different lifetimes.[112] The results of the work by Budde and co-workers support the latest interpretation.

Modeling of the dynamics of the multiphonon relaxation process has also played a key role in the understanding of the vibrational lifetime of hydrogen. The results by Gai and Voth and others show that the vibrational lifetime as well as the corresponding dominant decay channel can be obtained quite accurately using a perturbative calculation, involving Bloch–Redfield theory and MD simulations, in which the Si–H oscillator is treated quantum mechanically. Quantitative models explaining the large structural dependence of the vibrational lifetime require detailed knowledge of the local structure of the defects and the associated local phonons. The measured lifetimes provide an indispensable benchmark to develop more accurate calculations based on improved potential energy functions.

Future directions will focus on elucidating the strong structural dependence of the vibrational lifetime and energy transfer channels of the Si–H stretch mode. Temperature- and strain-dependent lifetime measurements will shed light on the preferential coupling between the Si–H oscillator and the bulk phonons. Two-color transient bleaching experiments will allow direct measurements of the energy transfer process between localized modes, enlightening the role of the bending mode in the decay process. Characterization and control of materials on the time scale associated with the fundamental vibration period of solid-state atomic motion will reveal insights into energy pathways, defect reactions, and complex formation. These exciting directions provide the promise of establishing a solid-state science involving quantum-level control.

ACKNOWLEDGMENTS

First and foremost, the authors wish to thank Michael Budde who, while visiting Vanderbilt University as a postdoctorate, conducted the vibrational lifetime measurements of bond-center hydrogen in silicon, raising the art of defect

Downloaded 24 May 2004 to 129.59.117.76. Redistribution subject to AIP license or copyright, see http://jap.aip.org/jap/copyright.jsp

spectroscopy to new heights. The authors are indebted to many colleagues with whom they have collaborated on various lifetime experiments of hydrogen- and deuterium-related modes in silicon. The groups by M. Stavola at Lehigh University and A. K. Ramdas at Purdue University performed high-resolution FTIR absorption spectroscopy in combination with samples with very low defect densities to measure the vibrational lifetime of a variety of H- and D-related defects in Si. J. C. Tully provided stimulating discussions on theoretical calculations of vibrational lifetimes. The authors are grateful to P. Guyot-Sionnest and Y. J. Chabal for letting them reproduce some of their exciting results obtained from hydrogenated Si surfaces. Their papers taught the authors a lot about vibrational energy relaxation of hydrogen on Si surfaces. The authors thank M. Rella, G. A. Voth, and J. L. Feldman for generously contributing figures for this article. The authors are indebted to the many postdoctorates and students who conducted vibrational lifetime measurements, including X. Zhang, C. Cheney Parks, B. Sun, and A. Fraser. The authors gratefully acknowledge the staff at the TJNAF FEL for providing them with high-quality beam time and W. M. Augustyniak for technical assistance. This work was supported in part by DOE through Grant No. DE-FG02-99ER45781 (C.W.M. and V.U.), ONR (C.W.M. and V.U.), NSF through Grant No. DMR-00-76027 (C.W.M.), and the Thomas F. and Kate Miller Jeffress Memorial Trust through Grant No. J-545 (C.W.M.).

[1] C. L. Tang and L. K. Cheng, *Fundamentals of Optical Parametric Processes and Oscillators* (Harwood Academic, Amsterdam, 1995).
[2] J.-Y. Zhang, J. Y. Huang, and Y. R. Shen, *Optical Parametric Generation and Amplification* (Harwood Academic, Amsterdam, 1995).
[3] W. B. Colson, E. D. Johnson, M. J. Kelley, and H. A. Schwettman, Phys. Today **55**, 35 (2002).
[4] G. R. Neil, C. L. Bohn, S. V. Benson, G. Biallas, D. Douglas, H. F. Dylla, R. Evans, J. Fugitt, A. Grippo, J. Gubeli, R. Hill, K. Jordan, R. Li, L. Merminga, P. Piot, J. Preble, M. Shinn, T. Siggins, R. Walker, and B. Yunn, Phys. Rev. Lett. **84**, 662 (2000).
[5] J. R. Engholm, U. Happek, and A. J. Sievers, Chem. Phys. Lett. **249**, 387 (1996).
[6] D. J. Myers, R. S. Urdahl, B. J. Cherayil, and M. D. Fayer, J. Chem. Phys. **107**, 9741 (1997).
[7] M. Broquier, H. Dubost, R. Kolos, J. Lefevre, A. Tramer, J. M. Berset, J. M. Ortega, and A. J. Sievers, Opt. Commun. **118**, 255 (1995).
[8] S. Woutersen, U. Emmerichs, H.-K. Nienhuys, and H. J. Bakker, Phys. Rev. Lett. **81**, 1106 (1998).
[9] B. Uebbing and A. J. Sievers, Phys. Rev. Lett. **76**, 932 (1996).
[10] M. Bonn, S. Woutersen, and H. J. Bakker, Opt. Commun. **147**, 138 (1998).
[11] Y. J. Chabal, Surf. Sci. Rep. **8**, 211 (1988).
[12] Y. J. Yan and S. Mukamel, J. Chem. Phys. **94**, 179 (1991).
[13] M. Bonn, M. J. Brugmans, A. W. Kleyn, R. A. van Santen, and H. J. Bakker, Phys. Rev. Lett. **76**, 2440 (1996).
[14] N. A. Kurnit, I. D. Abella, and S. R. Hartmann, Phys. Rev. Lett. **13**, 567 (1964); I. D. Abella, N. A. Kurnit, and S. R. Hartmann, Phys. Rev. **141**, 391 (1966).
[15] A. Tokmakoff, A. S. Kwok, R. S. Urdahl, R. S. Francis, and M. D. Fayer, Chem. Rev. Lett. **234**, 289 (1995).
[16] D. Zimdars, A. Tokmakoff, S. Chen, S. R. Greenfield, and M. D. Fayer, Phys. Rev. Lett. **70**, 2718 (1993).
[17] A. S. Barker, Jr. and A. J. Sievers, Rev. Mod. Phys. **47**, FS1 (1975).
[18] *Identification of Defects in Semiconductors: Semiconductors and Semimetals*, edited by M. Stavola (Academic, New York, 1999), Vol. 51B, Chap. 3, and references therein.
[19] S. J. Pearton, J. W. Corbett, and M. Stavola, *Hydrogen in Crystalline Semiconductors*, (Springer, Berlin, 1992), and references therein.
[20] *Hydrogen in Semiconductors II: Semiconductors and Semimetals*, edited by N. H. Nickel (Academic, New York, 1999), Vol. 61, and references therein.
[21] T.-C. Shen, C. Wang, G. C. Abeln, J. R. Tucker, J. W. Lyding, Ph. Avouris, and R. E. Walkup, Science **268**, 1590 (1995).
[22] K. Hess, L. F. Register, B. Tuttle, J. Lyding, and I. C. Kizilyalli, Physica E **3**, 1 (1998).
[23] B. N. J. Persson and Ph. Avouris, Surf. Sci. **390**, 45 (1997).
[24] E. T. Foley, A. F. Kam, J. W. Lyding, and Ph. Avouris, Phys. Rev. Lett. **80**, 1336 (1998).
[25] C. G. Van de Walle and W. B. Jackson, Appl. Phys. Lett. **68**, 2526 (1996).
[26] A. G. Redfield, IBM J. Res. Dev. **1**, 19 (1957).
[27] R. K. Wangsness and F. Bloch, Phys. Rev. **89**, 728 (1953).
[28] J. M. Jean, R. A. Friesner, and G. R. Fleming, J. Chem. Phys. **96**, 5827 (1992).
[29] F. E. Figueirido and R. M. Levy, J. Chem. Phys. **97**, 703 (1992).
[30] C. P. Slichter, *Principles of Magnetic Resonance* (Harper & Row, New York, 1963).
[31] M. Weissbluth, *Photon–Atom Interactions* (Academic, New York, 1989).
[32] R. Silbey and R. Wertheimer, Chem. Phys. Lett. **75**, 243 (1980).
[33] D. W. Oxtoby, Adv. Chem. Phys. **47**, 487 (1981).
[34] S. Velsko and D. W. Oxtoby, J. Chem. Phys. **72**, 2260 (1980).
[35] J. Chesnoy and G. M. Gale, Adv. Chem. Phys. **LXX**, 297 (1988).
[36] W. D. Partlow and H. W. Moos, Phys. Rev. **157**, 252 (1967).
[37] L. A. Riseberg and H. W. Moos, Phys. Rev. Lett. **19**, 1423 (1967).
[38] L. A. Riseberg and H. W. Moos, Phys. Rev. **174**, 429 (1968).
[39] H. W. Moos, J. Lumin. **1**, 106 (1970).
[40] M. J. Weber, Phys. Rev. B **8**, 54 (1973).
[41] M. D. Sturge, Phys. Rev. B **8**, 6 (1973).
[42] M. P. Miller and J. C. Wright, J. Chem. Phys. **71**, 324 (1979).
[43] T. T. Basiev, A. Y. Dergachev, Y. V. Orlowskii, and A. M. Prokhorov, J. Lumin. **53**, 19 (1992).
[44] G. Zhang, X. Ying, L. Yao, T. Chen, and H. Chen, J. Lumin. **59**, 315 (1994).
[45] Y. V. Orlovskii R. J. Reeeves, and R. C. Powell, Phys. Rev. B **49**, 3821 (1994).
[46] D. S. Tinti and G. W. Robinson, J. Chem. Phys. **49**, 3229 (1968).
[47] H. Dubost, L. Abouaf-Marguin, and F. Legay, Phys. Rev. Lett. **29**, 145 (1972).
[48] L. Abouaf-Marguin, H. Dubost, and F. Legay, Chem. Phys. Lett. **22**, 603 (1973).
[49] E. J. Heilweil, M. P. Casassa, R. R. Cavanagh, and J. C. Stephenson, Chem. Phys. Lett. **117**, 185 (1985).
[50] M. P. Casassa, E. J. Heilweil, J. C. Stephenson, and R. R. Cavanagh, J. Chem. Phys. **84**, 2361 (1986).
[51] D. Kuszner and N. Schwentner, J. Chem. Phys. **98**, 6965 (1993).
[52] R. Kubo and Y. Toyozawa, Prog. Theor. Phys. **13**, 160 (1955).
[53] Y. E. Perlin, Sov. Phys. Usp. **6**, 542 (1964).
[54] T. Miyakawa and D. L. Dexter, Phys. Rev. B **1**, 2961 (1970).
[55] F. K. Fong, S. L. Naberhuis, and M. M. Miller, J. Chem. Phys. **56**, 4020 (1972).
[56] S. H. Lin, J. Chem. Phys. **65**, 1053 (1976).
[57] S. H. Lin, in *Radiationless Transitions*, edited by S. H. Lin (Academic, New York, 1980).
[58] B.-Z. Zhang, Y.-X. Li, M.-R. Lin, and W.-J. Chen, Chin. Phys. **10**, 876 (1990).
[59] R. Englman, *Nonradiative Decay of Ions and Molecules in Solids* (North-Holland, Amsterdam, 1979).
[60] F. K. Fong, *Theory of Molecular Relaxation* (Wiley, New York, 1975).
[61] S. A. Egorov and J. L. Skinner, J. Chem. Phys. **103**, 1533 (1995).
[62] A. Nitzan and J. Jortner, Mol. Phys. **25**, 713 (1973); A. Nitzan, S. Mukamel, and J. Jortner, J. Chem. Phys. **60**, 3929 (1974).
[63] R. P. Feynman and A. R. Hibbs, *Quantum Mechanics and Path Integrals* (McGraw-Hill, New York, 1965).
[64] N. Bloembergen, *Nonlinear Optics* (Benjamin, New York, 1963).
[65] S. Mukamel, *Principles of Nonlinear Optical Spectroscopy* (Oxford, New York, 1995).
[66] Y. R. Shen, *The Principles of Nonlinear Optics* (Wiley, New York, 1984).
[67] G. Lüpke, Surf. Sci. Rep. **35**, 75 (1999).
[68] J. F. McGilp, J. Phys. D **29**, 1812 (1995).
[69] T. F. Heinz, in *Nonlinear Surface Electromagnetic Phenomena*, edited by E. Ponath, G. I. Stegeman (Elsevier, Amsterdam, 1991), Chap. 5, p. 353.
[70] See, for example, review articles, Y. R. Shen, in *Proceedings of the International School of Physics "Enrico Fermi,"* Course CXX, edited by T. Hänsch and M. Inguscio (North-Holland, Amsterdam, 1994) p. 139; J. Y.

Downloaded 24 May 2004 to 129.59.117.76. Redistribution subject to AIP license or copyright, see http://jap.aip.org/jap/copyright.jsp

Huang and Y. R. Shen, in *Laser Spectroscopy and Photochemistry on Metal Surfaces*, edited by H. L. Dai and W. Ho (World Scientific, Singapore, 1995), p. 5.
[71] H. W. K. Tom, Ph.D. thesis, University of California, Berkeley (1984).
[72] X. D. Zhu, H. Suhr, and Y. R. Shen, Phys. Rev. B **35**, 3047 (1987).
[73] J. H. Hunt, P. Guyot-Sionnest, and Y. R. Shen, Chem. Phys. Lett. **133**, 189 (1987).
[74] A. L. Harris, C. E. Chidsey, N. J. Levinos, and N. D. Loiacono, Chem. Phys. Lett. **141**, 350 (1987).
[75] D. D. Dlott, in *Laser Spectroscopy of Solids II*, edited by W. M. Yen (Springer, Berlin, 1989), Chap. 5.
[76] H. J. Stein, Phys. Rev. Lett. **43**, 1030 (1979).
[77] N. N. Gerasimenko, M. Rolle, L. J. Cheng, Y. H. Lee, J. C. Corelli, and J. W. Corbett, Phys. Status Solidi B **90**, 689 (1978).
[78] B. N. Mukashev, K. H. Nussupov, and M. F. Tamendarov, Phys. Lett. **72A**, 381 (1979).
[79] G. R. Bai, M. W. Qi, L. M. Xie, and T. S. Shi, Solid State Commun. **56**, 277 (1985).
[80] T. S. Shi, L. M. Xie, G. R. Bai, and M. W. Qi, Phys. Status Solidi B **131**, 511 (1985).
[81] X. T. Meng, Y. C. Chang, and Y. D. Fan, Phys. Status Solidi A **101**, 619 (1987).
[82] M. Budde, G. Lüpke, C. Parks Cheney, N. H. Tolk, and L. C. Feldman, Phys. Rev. Lett. **85**, 1452 (2000).
[83] Stein observed an absorption line at 1990 cm^{-1} after implantation of protons into Si at 80 K; M. Budde *et al.* recently showed that this line originates from $H_{BC}^{(+)}$. (see Ref. 85).
[84] M. Budde, Ph.D. thesis, Aarhus University, Denmark (1998).
[85] Y. V. Gorelkinskii, in *Hydrogen in Semiconductors II: Semiconductors and Semimetals*, edited by N. H. Nickel (Academic, New York, 1999), Vol. 61, Chap. 3.
[86] B. Holm, K. Bonde Nielsen, B. Bech Nielsen, J. Hansen, E. Andersen, and J. U. Andersen, Phys. Rev. Lett. **66**, 2360 (1991); K. Bonde Nielsen *et al.*, Phys. Rev. B **60**, 1716 (1999).
[87] S. K. Estreicher, Mater. Sci. Eng., R. **14**, 319 (1995).
[88] B. N. Mukashev, M. F. Tamendarov, S. Z. Tokmoldin, and V. V. Frolov, Phys. Status Solidi A **91**, 509 (1985).
[89] See e.g. B. H. Bransden, and C. J. Joachain, *Physics of Atoms and Molecules* (Longman Scientific & Technical, Harlow, 1983).
[90] J. D. Holbech, B. Bech Nielsen, R. Jones, P. Sitch, and S. Öberg, Phys. Rev. Lett. **71**, 875 (1993).
[91] M. Budde, B. Bech Nielsen, P. Leary, J. Goss, R. Jones, P. R. Briddon, S. Öberg, and S. J. Breuer, Phys. Rev. B **57**, 4397 (1998).
[92] P. Stallinga, P. Johannesen, S. Herstrøm, B. Bech Nielsen, and J. R. Byberg, Phys. Rev. B **58**, 3842 (1998).
[93] B. Bech Nielsen, L. Hoffmann, and M. Budde, Mater. Sci. Eng., B **36**, 259 (1996).
[94] M. Budde, G. Lüpke, E. Chen, X. Zhang, N. H. Tolk, L. C. Feldman, E. Tarhan, A. K. Ramdas, and M. Stavola, Phys. Rev. Lett. **87**, 145501 (2001).
[95] M. Suezawa, Phys. Rev. B **63**, 035203 (2001).
[96] G. Lüpke, X. Zhang, B. Sun, A. Fraser, N. H. Tolk, and L. C. Feldman, Phys. Rev. Lett. **88**, 135501 (2002).
[97] C. Flensburg and R. F. Stewart, Phys. Rev. B **60**, 284 (1999).
[98] J. W. Lyding, K. Hess, and I. C. Kizilyalli, Appl. Phys. Lett. **68**, 2526 (1996).
[99] T. Vondrak and X.-Y. Zhu, Phys. Rev. Lett. **82**, 1967 (1999).
[100] J. Chevallier, M. Barbe, E. Constant, D. Loridant-Bernard, and M. Constant, Appl. Phys. Lett. **75**, 112 (1999).
[101] P. Guyot-Sionnest, P. Dumas, Y. J. Chabal, and G. S. Higashi, Phys. Rev. Lett. **64**, 2156 (1990); P. Guyot-Sionnest, P. Dumas, and Y. J. Chabal, J. Electron Spectrosc. Relat. Phenom. **54/55**, 27 (1990).
[102] A. H. Mahan and M. Vanecek, AIP Conf. Proc. **234**, 195 (1991).
[103] D. Kwon, J. D. Cohen, B. P. Nelson, and E. Iwaniczko, Mater. Res. Soc. Symp. Proc. **377**, 301 (1995).
[104] G. Ganguly, I. Sakata, H. Okushi, and A. Matsuda, Jpn. J. Appl. Phys., Part 2 **34**, L277 (1995).
[105] P. Stradins and H. Fritzsche, J. Non-Cryst. Solids **198-200**, 432 (1996).
[106] Y. Lee, L. Jiao, J. Hoh, H. Fujiwara, Z. Lu, R. W. Collins, and C. R. Wronski, Mater. Res. Soc. Symp. Proc. **467**, 747 (1997).
[107] D. L. Staebler and C. R. Wronski, Appl. Phys. Lett. **31**, 292 (1977).
[108] H. Fritzsche, Mater. Res. Soc. Symp. Proc. **467**, 19 (1997).
[109] M. Stutzmann, Mater. Res. Soc. Symp. Proc. **467**, 37 (1997).
[110] H. M. Branz, Phys. Rev. B **59**, 5498 (1999).
[111] Z. Xu, P. M. Fauchet, C. W. Rella, H. A. Schwettman, and C. C. Tsai, J. Non-Cryst. Solids **198-200**, 11 (1996).
[112] C. W. Rella, M. van der Voort, A. V. Akimov, A. F. G. van der Meer, and J. I. Dijkhuis, Appl. Phys. Lett. **75**, 2945 (1999).
[113] M. van der Voort, C. W. Rella, L. F. G. van der Meer, A. V. Akimov, and J. I. Dijkhuis, Phys. Rev. Lett. **84**, 1236 (2000).
[114] J. Fabian and P. B. Allen, Phys. Rev. Lett. **77**, 3839 (1996).
[115] S. R. Bickham and J. L. Feldman, Phys. Rev. B **57**, 12234 (1998).
[116] M. Maroniov and N. Zotov, Phys. Rev. B **55**, 2938 (1997).
[117] B. Guillot and Y. Guissani, Phys. Rev. Lett. **78**, 2401 (1997).
[118] S. R. Bickham and J. L. Feldman, Philos. Mag. B **77**, 513 (1998).
[119] E. J. Heilweil, M. P. Casassa, R. R. Cavanagh, and J. C. Stephenson, J. Chem. Phys. **81**, 2856 (1984).
[120] E. J. Heilweil, M. P. Casassa, R. R. Cavanagh, and J. C. Stephenson, J. Chem. Phys. **82**, 5216 (1985).
[121] E. J. Heilweil, M. P. Casassa, R. R. Cavanagh, and J. C. Stephenson, J. Chem. Phys. **92**, 6099 (1988).
[122] A. L. Harris and N. J. Levinos, J. Chem. Phys. **90**, 3878 (1989).
[123] A. L. Harris, L. Rothberg, L. H. Dubois, N. J. Levinos, and L. Dhar, Phys. Rev. Lett. **64**, 2086 (1990).
[124] J. D. Beckerle, M. P. Casassa, R. R. Cavanagh, E. J. Heilweil, and J. C. Stephenson, Phys. Rev. Lett. **64**, 2090 (1990).
[125] H. C. Chang and G. E. Ewing, J. Phys. Chem. **94**, 7635 (1990).
[126] H. Kobayashi, K. Edamoto, M. Onchi, and M. Nishijima, J. Chem. Phys. **78**, 7429 (1983); H. Froitzheim, U. Köhler, and H. Lammering, Surf. Sci. **149**, 537 (1985).
[127] P. Dumas, Y. J. Chabal, and G. S. Higashi, Phys. Rev. Lett. **65**, 1124 (1990).
[128] J. C. Tully, Y. J. Chabal, K. Raghavachari, J. M. Bowman, and R. R. Lucchese, Phys. Rev. B **31**, 1184 (1985).
[129] P. Guyot-Sionnest, P. H. Lin, and E. M. Hiller, J. Chem. Phys. **102**, 4269 (1995).
[130] Y. J. Chabal, Surf. Sci. **168**, 594 (1986).
[131] B. J. Min, Y. H. Lee, C. Z. Wang, C. T. Chan, and K. M. Ho, Phys. Rev. B **46**, 9677 (1992).
[132] H. Gai and G. A. Voth, J. Chem. Phys. **99**, 740 (1993).
[133] P. Guyot-Sionnest, Phys. Rev. Lett. **66**, 1489 (1991).
[134] P. Guyot-Sionnest, Phys. Rev. Lett. **67**, 2323 (1991).
[135] V. A. Ermorshin, A. K. Kazansky, K. S. Smirnov, and D. Bougeard, J. Chem. Phys. **105**, 9371 (1996).
[136] E. L. Sibert III, W. P. Reinhardt, and J. T. Hynes, J. Chem. Phys. **81**, 1115 (1984).

Downloaded 24 May 2004 to 129.59.117.76. Redistribution subject to AIP license or copyright, see http://jap.aip.org/jap/copyright.jsp